NAVAL POSTGRADUATE SCHOOL
Monterey, California

DTIC QUALITY INSPECTED

Processing of Second Order Statistics via Wavelet Transforms

by

Ralph D. Hippenstiel
Monique P. Fargues
Nabil H. Khalil
Howard F. Overdyk

February 1998

Prepared for: Space and Naval Warfare Systems Command

19980317 051

NAVAL POSTGRADUATE SCHOOL
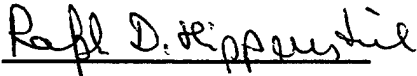### Monterey, California
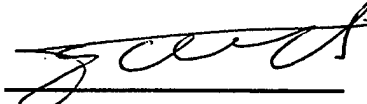
CAPT James Burin
Superintendent

R. Elster
Provost

This report was sponsored by the Space and Naval Warfare Systems Command.

Approved for public release; distribution is unlimited.
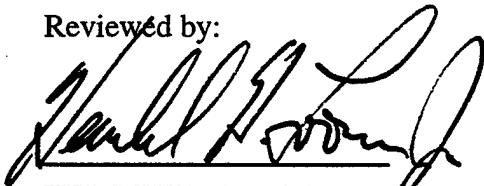
The report was prepared by:

RALPH D. HIPPENSTIEL
Associate Professor
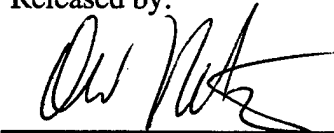Department of Electrical and
Computer Engineering

MONIQUE P. FARGUES
Associate Professor
Department of Electrical and
Computer Engineering

Reviewed by:

HERSCHEL H. LOOMIS, JR.
Chairman
Department of Electrical and
Computer Engineering

Released by:

DAVID W. NETZER
Associate Provost and
Dean of Research

REPORT DOCUMENTATION PAGE

Public reporting burden for the collection of information is estimated to average 1 hour per response, including the time for reviewing instructions, searching existing data sources, gathering and maintaining the data needed, and completing and reviewing the collection of information. Send comments regarding this burden estimate or any other aspect of this collection of information, including suggestions for reducing this burden to Washington Headquarters Services, Directorate for Information Operations and Reports, 1215 Jefferson Davis Highway, Suite 1204, Arlington VA 22202-4302, and to the Office of Management and Budget, Paperwork Reduction Project (0704-0188), Washington DC 20503.

1. AGENCY USE ONLY (Leave blank)	2. REPORT DATE February 20, 1998	3. REPORT TYPE AND DATES COVERED July 1, 1996 - December 31, 1997

4. TITLE AND SUBTITLE	5. FUNDING NUMBERS
Processing of Second Order Statistics via Wavelet Transform	MIPR 97245T

6. AUTHOR(S)

Ralph D. Hippenstiel, Monique Fargues, Nabil H. Khalil, and Howard F. Overdyk

7. PERFORMING ORGANIZATION NAME(S) AND ADDRESS(ES)	8. PERFORMING ORGANIZATION REPORT NUMBER
Department of Electrical and Computer Engineering Naval Postgraduate School Monterey, CA 93943-5000	NPS-EC-98-003

9. SPONSORING/MONITORING AGENCY NAME(S) AND ADDRESS(ES)	10. SPONSORING/MONITORING AGENCY REPORT NUMBER
ISC, WF4/I2PO 4101 Pleasant Valley Road Chantilly, VA 20151	

11. SUPPLEMENTARY NOTES

The views expressed in this report are those of the author and do not reflect the official policy or position of the Department of Defense or the United States Government.

12a. DISTRIBUTION/AVAILABILITY STATEMENT	12b. DISTRIBUTION CODE
Approved for public release; distribution is unlimited.	A

13. ABSTRACT (Maximum 200 words)

Research was conducted to evaluate the feasibility of wavlet transforming second order statistics. To identify the modulation type and to extract signal modulation parameters of frequency hopped signals wavelet functions are applied to the 2-dimensional instantaneous correlation function. Parameters of interest are switching times and hop frequencies. The characteristics of the wavelet transform of the correlation function is derived. The wavelet transform is applied along the delay and the time axes. Processing along the delay axis allows the identification of frequency hopped signals and estimation of frequencies and switching times. Processing along the time axis allows detection of the transition times of frequency and time hopped signals.

14. SUBJECT TERMS Wavelets, signal processing, non-stationary correlation function, digital communication signals, identification, demodulation, detection, frequency hopping, spread spectrum			15. NUMBER OF PAGES 73
			16. PRICE CODE

17. SECURITY CLASSIFICATION OF REPORT UNCLASSIFIED	18. SECURITY CLASSIFICATION OF THIS PAGE UNCLASSIFIED	19. SECURITY CLASSIFICATION OF ABSTRACT UNCLASSIFIED	20. LIMIITATION OF ABSTRACT SAR

Table of Content

Summary:

Research was conducted to evaluate the feasibility of wavelet transforming second order statistics. To identify the modulation type and to extract signal modulation parameters of frequency hopped signals the wavelet transform is applied to the 2-dimensional instantaneous correlation function. Parameters of interest are switching times and hop frequencies. The characteristics of the wavelet transform of the correlation function are derived. The wavelet transform of the correlation function can replace the requirement to Fourier transform the complete correlation surface with a Fourier transform once per hop to estimate the hop frequency of a given hop. Wavelet processing is applied along the delay and time axes.

Processing along the delay axis leads to the following conclusions:
- To perform visual identification an SNR of 3 dB is required.
- For frequencies larger than 1/16 of the sampling rate the hop frequencies can be estimated with a success rate of 100% for SNR levels of 0 dB or better.
- To estimate the hop times with an accuracy of 12 to 17.5 % an SNR of 6 dB or better is required.
- If the true start and stop time are used we can obtain an improvement of the spectral estimation performance by about 2 dB.

- Processing along the time axis allows detection of the transition times of frequency and time hopped signals. The current implementation is limited to work with one transition per observation interval but permits robust detection at an SNR level of 3 dB.

1. Introduction

This work focuses on the wavelet transform of the second order moment function to enhance detection and classification of frequency hopped signals. There are four useful and important representations when dealing with non-stationary processes:

i) the temporal correlation function,

ii) the ambiguity function,

iii) the spectral correlation function, and

iv) the time frequency distribution.

Any of the four representations can be reached from any other representation by performing a one or two-dimensional Fourier transforms (Fig. 1).

We will use the temporal correlation function as the starting point and examine the two domains reachable by a one-dimensional Fourier transform. If we Fourier transform over the delay or time axis of the correlation function, we obtain the Wigner-Ville Distribution or the ambiguity function, respectively. In all discussions we use an approximation for the true correlation function. If the expectation operator is left out then

$R_x(t,\tau) = E[x^*(t-\tau/2)\, x(t+\tau/2)]$ becomes $x^*(t-\tau/2)\, x(t+\tau/2)$.

This is not an unusual approximation since we cannot apply an expectation operator to the data nor can we apply time domain averaging. Our work will focus on this correlation function which is called the instantaneous correlation function. In particular we will replace the traditional Fourier transform with the wavelet transform. Chapters 1-2 deal with general background, chapters 3-5 address transformation over the delay axis, while chapter 6 focuses on the transformation over the time axis.
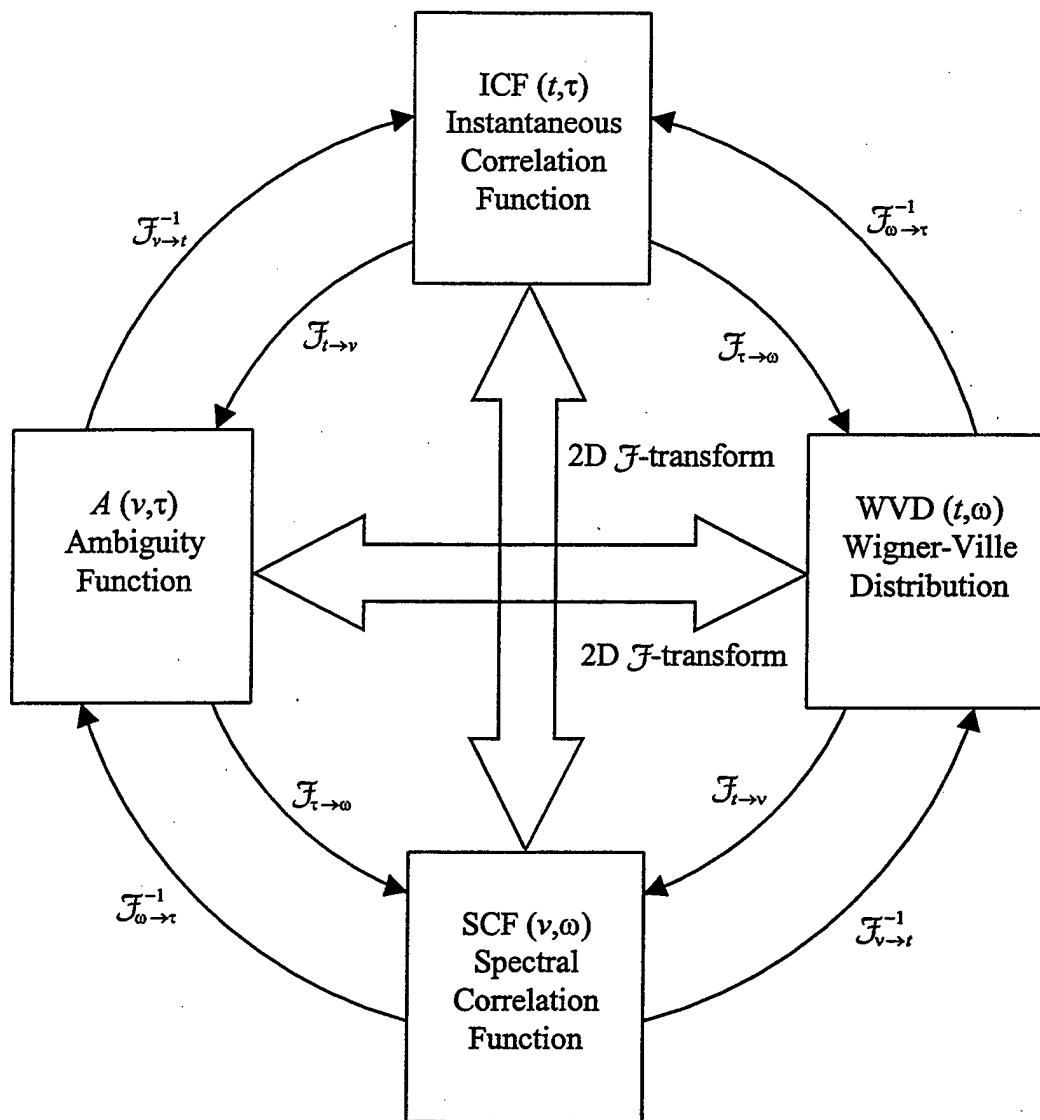
Figure 1: Time frequency representation.

2. General Background

In some applications there is the desire to intercept digital communication signals. The task of intercepting a communication signal can be summarized by i) detect the signal's presence, ii) classify the modulation type, iii) estimate the reception control parameters, iv) decode the data, and v) decrypt the information content. The process can be stopped at any intermediate step.

Spread spectrum (SS) modulation is a widely used modulation technique. Frequency hopping (FH) is a modulation subset of SS, and is primarily addressed in this report.

Many signal processing tools are available to help to achieve the tasks listed above. In particular, correlation processing and wavelet analysis of the time domain data have been used for the interception task. In this work we will address the merging of wavelet and correlation concepts to enhance detection, classification and signal parameter estimation. For the interested reader an extensive reference section [1-64] is provided.

The FH signal is a non-stationary process having a two-dimensional correlation function. Application of wavelet analysis to correlation functions is a new area and is still in the exploratory stage. This work assesses wavelet processing of the correlation function along the delay and time axis.

3

2.1 INTERCEPTION OF DIGITAL COMMUNICATION SIGNALS

Interception of communication signals is of interest to a wide range of applications in surveillance, intelligence, reconnaissance, geo-location, spectral monitoring and jamming [1]. Digital communication systems can use a large number of modulation techniques (i.e., ASK, BPSK, BFSK, QAM, MPSK ,MFSK , Spread Spectrum). Interception of digital communication signals consists of detection, classification, parameter estimation, decoding, and decryption.

A large number of publications address the interception of digital communication signals. Signal processing is used for the interception and can be grouped into the following approaches:

- Second order moments: Spectral analysis and correlation analysis

- Linear: Linear transforms including the wavelet transform

- Nonlinear: Higher-order spectra, spectral correlation, and cyclic-feature processing

- Other: Eigen-analysis, singular-value decomposition, and stochastic resonance.

Demodulation of ASK, QAM, BPSK, and DPSK are addressed in [2-14,17,32]. Time domain correlation and Spectral correlation are used on FSK related problems in [2,33], higher-order moments are used in [3], and wavelet analysis is used in [5,17,56,65].

2.2 Spread Spectrum Signals

Interception of spread spectrum signals is addressed in [17-31]. These techniques differ mainly in the bandwidth of the interception filter(s) relative to the bandwidth of the FH signal and the number of parallel channels relative to the number of hopping frequencies.

2.3 FOURIER ANALYSIS, TIME FREQUENCY DISTRIBUTIONS AND WAVELETS

Signal analysis treats time signals as a linear combination of elementary basis functions.

Well-known examples are the Shannon, the Karhunen-Loeve, the Gram-Schmidt expansion, the Eigen-decomposition, and the Fourier analysis. We will review the Fourier analysis, Time Frequency Distributions and Wavelet analysis [41,52-58,61].

2.4 Fourier Transform

The Fourier transform (FT) is the most popular signal decomposition [36]. It is used to decompose stationary signals into sinusoidal or complex exponential components. A non-periodic continuous time signal, x(t), can be represented as

$$x(t) = \int_{-\infty}^{\infty} X(f) \, e^{j2\pi ft} \, df$$
$$\text{with} \qquad\qquad (1)$$
$$X(f) = \int_{-\infty}^{\infty} x(t) \, e^{-j2\pi ft} \, dt \quad ;$$

where the signal and its transform are continuous functions of time and frequency, respectively.

2.5 Short Time Fourier Transform

To track time evolution the short time Fourier transform (STFT) was developed. The STFT windows the signal around a given time instant, performs the frequency domain analysis, and repeats the process at other time instants of interest. The basic assumption is that the windowed signal has a non-time-varying spectrum (local stationarity) within the time window. The STFT for a continuous signal x(t) is given by

$$X(f,\tau) = \int_{-\infty}^{\infty} x(t) \, w^*(t-\tau) \, e^{-j2\pi ft} \, dt. \qquad (2)$$

where w(t) is the window function. $X(f,\tau)$ is the spectral description of x(t), * denotes conjugation and the time window is centered at τ. If the window has a Gaussian shape, the

STFT is called the Gabor transform. Time and frequency localization are controlled by the effective window duration. The STFT has a fixed-time and fixed-frequency resolution, which results in a uniform tiling of the time-frequency plane. For discrete time signals the STFT is defined as

$$X(k,m) = \sum_{-\infty}^{\infty} x(n) \ w(m-n) \ e^{-j2\pi kn/M}$$
$$where \ k = 0,1,2,..,M-1.$$

(3)

2.6 Discrete Fourier Transform

A finite-length non-periodic discrete signal has a continuous-frequency-domain representation. The discrete Fourier transform (DFT) and its fast implementation, the fast Fourier transform (FFT), use a finite integration time. For digital signal processing it is convenient to represent the process by its discrete-frequency samples. This leads to the discrete Fourier transform (DFT). The DFT pair is given by

$$x(n) = 1/N \sum_{k=0}^{N-1} X(k) \ e^{j2\pi kn/N}$$
$$X(k) = \sum_{n=0}^{N-1} x(n) \ e^{-j2\pi kn/N} \ ; \ for \ n,k = 0,1,..,N-1.$$

(4)

The DFT requires N^2 complex multiplication operations and $N(N-1)$ complex additions. The fast Fourier transform (FFT) implements the DFT with fewer multiplications. The FFT has computation complexity (number of multiplications) of $N/2 \ \log_2 N$. Time or frequency uncertainty can be reduced by using overlapping techniques [20].

2.7 Time Frequency Distributions

A Time Frequency Distribution (TFD) [38] can describe non-stationary signals by displaying the energy density as a function of time and frequency. The most popular TDF is the Wigner-Ville Distribution (WVD) [15,38,39,40]. The WVD of the signal s(t) is defined by:

$$WVD_S\ (t,\omega)\ =\ \int_{-\infty}^{\infty} s^*(t-\tau/2)\ s(t+\tau/2)\ e^{-j\omega\tau}\ d\tau;\qquad (5)$$

where $\omega = 2\pi f$. The WVD of the sum of two signals (i.e., $s(t) = s_1(t) + s_2(t)$) is given by

$W(t,\omega) = W_{11}(t,\omega) + W_{22}(t,\omega) + W_{12}(t,\omega) + W_{21}(t,\omega)$, where

$$W_{ij}\ (t,\omega)\ =\ \frac{1}{2\pi}\int_{-\infty}^{\infty} s_i^*(t-\tau/2)\ s_j(t+\tau/2)\ e^{-j\omega\tau}\ d\tau\qquad (6)$$

is a cross term. The cross term is complex-valued, but $W_{12} = W_{21}^*$ and hence

$W_{12}(t,\omega) + W_{21}(t,\omega)$ is real and $W(t,\omega) = W_{11}(t,\omega) + W_{22}(t,\omega) + 2\,Re\,[W_{12}(t,\omega)]$, where

the cross term $2\,Re\,[W_{12}(t,\omega)]$ is an interference term. Window functions can be chosen to

improve the WVD by minimizing cross terms.

2.8 Wavelets

Wavelet analysis is a new approach to represent non-stationary signals. In the following discussion we introduce wavelet analysis concepts. The function f(t) may be expressed as

$$f(t)\ =\ \sum_k a_k\ v_k(t)\ ;$$
$$with$$
$$a_k\ =\ <f(t),v_k(t)>\qquad\qquad (7)$$
$$=\ \int_{-\infty}^{\infty} f(t)\ v_k(t)\ dt\ ;$$

where the set $v_k(t)$ typically forms an ortho-normal set and $<\,>$ notation denotes an inner

product, i.e., a projection of the time data onto the kth basis function.

There are different types of wavelets; orthogonal, non-orthogonal, and bi-orthogonal wavelets. The Daubechies family, Symmlet, Coiflet, and Meyer wavelets are examples of orthogonal wavelets, while the Morlet wavelet is an example of a non-orthogonal wavelet [16,34,35,37,42-47].

2.9 Continuous Wavelet Transform

The continuous wavelet transform (CWT) forms the mathematical basis for wavelet analysis. In the wavelet analysis all basis functions can be generated from a single function called the mother wavelet, which is usually denoted by $\psi(t)$. The other wavelets can be generated using two distinct operations; scaling and translation. Scaling is the dilation or compression of the wavelet function according to a specific scaling value. The scale is denoted by s. The translation allows shifting of the (scaled) wavelet to a desired position in time. This shift is denoted by a. The scaled and translated wavelet is denoted by

$$\psi_{s,a}(t) = 1/\sqrt{s} \ \psi((t-a)/s);$$

where $\sqrt{s}$ is a normalization factor. The integral form of CWT of the finite energy signal f(t) with respect to the wavelet function $\psi(t)$ is given by [42,46]

$$W_f(s,a) = \int_{-\infty}^{\infty} f(t) \ \psi_{s,a}(t) \ dt$$
$$= 1/\sqrt{s} \int_{-\infty}^{\infty} f(t) \ \psi((t-a)/s) \ dt. \qquad (9)$$

The wavelet analysis computes inner products of the signal and the wavelet functions. We can also interpret the wavelet analysis as a linear operation which transforms the signal using modified kernel functions. The kernel of the transform is the mother wavelet, and the

modifications are the scaling and translation operations [44,45]. The wavelet operation can be interpreted as a bandpass function which implies that the wavelet must be an oscillatory function.

2.10 Scalogram

Using the scalogram, a signal $f(t)$ is characterized by the distribution of $|W_f(s,a)|^2$ over the time-scale plane. The quantity $|W_f(s,a)|^2$ may be viewed as a spectral density in units of power per scale [44]. Consequently, the scalogram represents the power spectral density of the signal over the time-scale plane. The quantity

$$\frac{1}{C_\psi s^2} \int_{-\infty}^{\infty} |W_f(s,a)|^2 \, da$$

represents the portion of the signal energy contained within the scale s. Here

$$C_\psi = \int_{-\infty}^{\infty} \frac{|\Psi(\omega)|^2}{|\omega|} \, d\omega \, < \, \infty \, ;$$

and $\Psi(\omega)$ is the Fourier transform of $\psi(t)$. This fact is exploited in identifying the scale for each frequency hop. In summary, the CWT is a linear, time-shift-invariant, time-scaling-invariant, and frequency-scaling-invariant operator.

2.11 Discrete Wavelet Transform

The CWT is defined by an integral transform over continuous variables in the scale s and the time shift a. In practice a discrete grid for s and a is used. A widely accepted discretization is to specify $s = s_o^m$ and $k = n a_o s_o^m$, where m and n are integers, $s_0 > 1$, and $a_0 > 0$ [45]. Furthermore, if we select $s_0 = 2$ and $a_0 = 1$ we obtain the well-known dyadic wavelet sampling (tiling) grid. Hence the scaled and translated wavelet indexed by m and n is given by

$$\psi_{m,n}(t) = 2^{-m/2} \psi(2^{-m}t - n).$$

We will briefly introduce the WT from the perspective of the multi-resolution (MR) analysis. The signal (or the time function) f(t) is expanded in terms of the wavelet functions. These wavelets have a frequency bandpass shape, so they result in a set of successive details of the signal. For the approximation we need a special basis, called the scaling function $\phi(t)$, which is not a wavelet. It has a low pass frequency behavior and performs averaging. The discrete wavelet synthesis equation is given by

$$f(t) = \sum_{k=-\infty}^{\infty} c(k)\phi_k(t) + \sum_{j=0}^{\infty} \sum_{k=0}^{\infty} d(j,k)\psi_{j,k}(t),$$

where j and k are integers, the coefficients c(k) constitute the coefficients of the approximation, while d(j,k) constitutes the coefficients of the added details or equivalently the fine resolutions [47]. If the wavelets and the associated scaling functions form an ortho-normal set of basis functions the coefficients are given by $c(k) = <f(t), \phi_k(t)>$, and $d(j,k) = <f(t), \psi_{j,k}(t)>$. Here $\phi(t)$ is a lowpass function whose frequency response is the same as the frequency response of $\psi(t)$ except that the frequency center of the bandpass filter is shifted to baseband (i.e., centered at DC).

2.12 Scaling and Wavelet Equations

The Multi-resolution subspace representation leads to a method to formulate two equations in terms of the unknown scaling and wavelet functions:

$$\phi(t) = \sqrt{2} \sum_{k} h_0(k) \, \phi(2t-k).$$

This equation includes two different scales of the scaling function and is known as the scaling or dilation equation. The coefficients $h_0(n)$ are called the scaling filter coefficients. We also have

$$\psi(t) = \sqrt{2} \sum_{k} h_1(k) \, \phi(2t-k).$$

which is called the wavelet equation. The coefficients $h_1(n)$ are the wavelet filter coefficients [42,47].

For discrete data the filter-bank concept leads to a simple method for computing the wavelet coefficients. The wavelet function is replaced by the coefficients of the wavelet filter $h_1(n)$ and the scaling function is replaced by the coefficients of the scaling filter $h_0(n)$. In [42,46,47], the following two recursive equations are obtained:

$$c(j,k) = \sum_{m} h_0(m-2k) \, c(j+1,m)$$
$$d(j,k) = \sum_{m} h_1(m-2k) \, c(j+1,m) \, .$$

These two recursive equations enable us to compute the jth scale wavelet transform and is known as Mallat's algorithm [46].

2.13 Daubechies Wavelet Family

The Daubechies wavelet family is a compactly supported ortho-normal set of wavelet

functions [42]. The Daubechies wavelet are obtained by solving the scaling and wavelet equations. An additional set of constraints is applied to satisfy the maximum number of vanishing moments for each wavelet. This report, and the Matlab wavelet toolbox [59], uses the notation that a Daubechies wavelet of order N has 2N coefficients. The wavelet of order N has finite support over [0,2N-1], or equivalently the corresponding FIR filter has 2N multipliers. The number of vanishing moments is an indication of the smoothness of the wavelet filter. The number of vanishing moments implies the number of zeros of $\Psi(\omega)$ at $\omega = \pi$. The higher the order the longer and smoother the Daubechies filter will be.

3. WAVELET TRANSFORMS AND CORRELATION FUNCTIONS

Correlating two functions provides a measure of their similarity. The Wiener-Khinchin theorem relates the signal's auto-correlation function and power spectral density for a stationary process. Wavelet decomposition can be used to represent non-stationary signals over the time-scale plane. We will examine the wavelet transform of the correlation function as an alternative for non-stationary signal representation.

3.1 Correlation Functions

Depending on the underlying process, various definitions can be given to the auto-correlation function (ACF). The process may be deterministic, stochastic, stationary or non-stationary.

The ACF of a stochastic process is the correlation between two samples of the process taken at t_1 and t_2, and is defined as $R(t_1,t_2) = E\{x (t_1) x^*(t_2)\}$, where $E \{ \}$ is the expectation operator and $*$ stands for the complex conjugation. For a stationary (i.e., wide-sense stationary) process, $R(t_1,t_2)$ depends only on the time lag $\tau = t_1 - t_2$. The Wiener-Khinchin theorem defines the relationship between the correlation function and spectral density as

$S_{xx}(\omega) = \int R(\tau) \exp(-j \omega \tau) d\tau.$

3.2 The Instantaneous Correlation Function

The ACF of a deterministic or stochastic process is computed using time domain averaging or the expectation operator, respectively. This means that a smoothing process has to be applied to compute the correlation functions. The instantaneous correlation function (ICF) does not use an averaging operation. The instantaneous correlation function is simply defined as the product of two samples of the process. These two samples are drawn at two time instants centered about time t. The instantaneous correlation function $R^i(t,\tau)$ is defined as

13

$R^i(t,\tau) = x \, (t+\tau/2) \, x^* \, (t-\tau/2)$, where i stands for the instantaneous nature of the correlation function [49].

If x(t) is a sinusoidal signal then the multiplication to obtain the values of $R^i(t,\tau)$ generates cross terms in the ICF. For example, the real-valued sinusoidal signal

$x(t) = A \cos(\omega t)$ has an ACF given by $R(\tau) = A^2/2 \cos(\omega \tau)$, while the ICF is given by

$R^i(t,\tau) = A^2/2 \, [\cos(2\omega t's) + \cos(\omega \tau)]$.

The ACF of a single sinusoidal signal has only one component and no cross term, while the ICF has cross terms. If the signal x(t) is represented by its analytic form, say $x(t) = A \exp(j \omega t)$, then its ICF is given by $R^i(t,\tau) = A^2 \exp(j \omega \tau)$.

That is, the ICF of a single complex exponential signal has no cross term. To minimize cross terms from the negative frequency components we use the analytic form of the data [49].

3.3 WAVELET TRANSFORMS OF CORRELATION FUNCTIONS

The wavelet transform of the stochastic ACF of a stationary process is addressed in [48]. The wavelet transform of the ACF of a deterministic signal will have a similar expression. Let $W_{XX}(s,a)$ denote the wavelet transform of $R(\tau)$. Note, the subscript in $W_{XX}(s,a)$ stands for the wavelet transform of the ACF of x(t) in contrast to $W_X(s,a)$ which denotes the wavelet transform of x(t). The wavelet basis function is denoted by $g(\tau)$. The wavelet transformation will transform the lag variable τ to the shift variable a and the scale s. $W_{XX}(s,a)$,for positive s is given by:

$$W_{XX}(s,a) = \frac{1}{\sqrt{s}} \int_{-\infty}^{\infty} R(\tau) \, g^* \, \frac{(\tau-a)}{s} d\tau$$

$$= \sqrt{s} \int_{-\infty}^{\infty} S_{XX}(f) \, G^*(sf) \, e^{j2\pi fa} \, df.$$

14

This equation has the form of an inverse Fourier transform from the variable f to the variable a. We can write $W_{XX}(s,a) = \mathscr{F}^{-1}\{\sqrt{s}\ S_{XX}\ (F)\ G^*(sf)\}$ and deduce that the wavelet transform, at any scale s > 0, represents a linear filtering operation using a band pass filter whose impulse response is the (time-reversed) wavelet function at scale s. Equivalently, the filter has a frequency response given by the FT of the scaled wavelet.

The wavelet transform of the ACF, $R(\tau)$, of the stationary finite-energy signal x(t), gives a band pass filtered version of the power spectral density $S_{XX}(f)$ of this signal (up to a constant, $\sqrt{s}$, the band pass filter used dependents on the chosen wavelet function and scale.

3.4 The Wavelet Transform of the Instantaneous Correlation Function

The Wigner-Ville Distribution (WVD) is used to represent non-stationary processes. The WVD applies a one-dimensional Fourier transformation to the ICF. The Fourier transform takes the delay τ to the frequency f, leaving the global time variable t unchanged. This allows the display of the time evolution of the spectrum of the signal. For one-dimensional time signals, the one-dimensional wavelet transform carries out a transformation from one global time variable t to the two wavelet variables, the shift a and the scale s. Consequently, the signal is represented by a time-scale distribution in the wavelet domain. The wavelet domain is called the time-scale domain. For the two-dimensional surface, indexed by time t and the delay τ, we carry out the wavelet transformation along the delay axis. This permits a display as a function of time. Let $V_X(t,f)$ denote the WVD of the signal x(t),

$$V_X(t,f) = \int_{-\infty}^{\infty} x((t-\tau/2)\ x^*(t+\tau/2)\ e^{-j2\pi f\tau}\ d\tau$$

$$= \int_{-\infty}^{\infty} R'_X(t,\tau)\ e^{-j2\pi f\tau}\ d\tau\ ,$$

15

and let the Fourier transform of the wavelet basis function be given by

$$\mathcal{F}\left(g\left(\frac{\tau - a}{s}\right)\right) = s\ G(sf)\ e^{-j2\pi fa}$$

so

$$g\left(\frac{\tau - a}{s}\right) = \int_{-\infty}^{\infty} s\ G(sf)\ e^{-j2\pi fa}\ df\ ,$$

then using

$$W^{i}_{xx}(t;s,a) = \frac{1}{\sqrt{s}} \int_{-\infty}^{\infty} R_{X}(t,\tau)\ g^{*}\left(\frac{\tau - a}{s}\right) d\tau\ ;$$

we have

$$W^{i}_{xx}(t;s,a) = \sqrt{s} \int_{-\infty}^{\infty} G^{*}(sf)\ V_{X}(t,f)\ e^{j2\pi fa}\ df\ .$$

This equation is in the form of an inverse Fourier transform. $W_{xx}^{i}(t; s,a)$ and $\sqrt{s}\ G^{*}(sf)\ V_{x}(t,f)$ are a Fourier transform pair with respect to the variable a and f. This relation suggests that we can obtain a filtered version of the WVD by Fourier transforming $W_{xx}^{i}(t; s,a)$.

3.5 FREQUENCY HOPPED SIGNALS AND THEIR CORRELATION FUNCTIONS

Communication systems can utilize a large number of digital modulation techniques; spread spectrum modulation being one of them. Spread spectrum refers to any modulation scheme that produces a transmitted bandwidth much larger than the information bandwidth [50]. We will briefly address different digital modulation schemes and focus on frequency hopping.

16

3.6 SPREAD SPECTRUM COMMUNICATION SIGNALS

Spread spectrum (SS) communication signals are characterized by a wide transmission bandwidth and a low power spectral density [19, 50,51]. SS signals have two main advantages:

i) The message has a low probability of being intercepted (LPI) as a result of the wide frequency band and the low power spectral density of the signals.

ii) SS systems can reject jamming signals and allow users to share the same frequency band.

Among the different possible SS modulation formats, the following three are prevalent: Frequency Hopping (FH), Direct Sequence (DS) Modulation and Time Hopping (TH).

3.7 THE INSTANTANEOUS CORRELATION FUNCTION OF FREQUENCY HOPPED SIGNALS

Spread spectrum studies usually consider the FH signal as a stationary process [19, 50,64] even though the spectrum of the FH signal varies with each hop interval. The stationary correlation representation, using time averaging, is not suitable for this process.

One way to identify the FH signal is to monitor the time-frequency evolution of the signal. Hence, we need to keep the time dependency in the correlation representation. This is achieved by using the instantaneous correlation function (ICF).

The FH signal may be represented as successive intervals (i.e., hops) of single frequency complex exponential (Fig. 2a). The frequency within each interval (i.e., the hop frequency) is controlled by a random (but known to the user) sequence. We assume without loss of generality that any two successive hops will have different frequencies.

The frequency difference of adjacent hops will generate the patterns of the instantaneous correlation functions. The IFC for values of $|\tau| \leq T_h$ (i.e., allows correlating adjacent hops only) and using values of $(t+\tau/2)$ and $(t-\tau/2)$ such that the values are confined to be within the
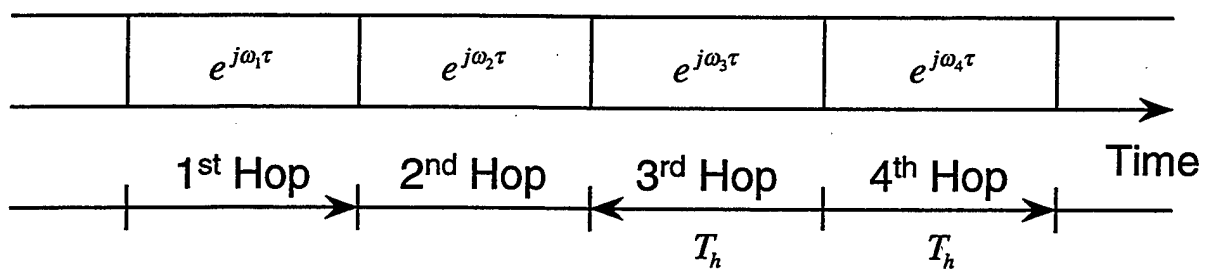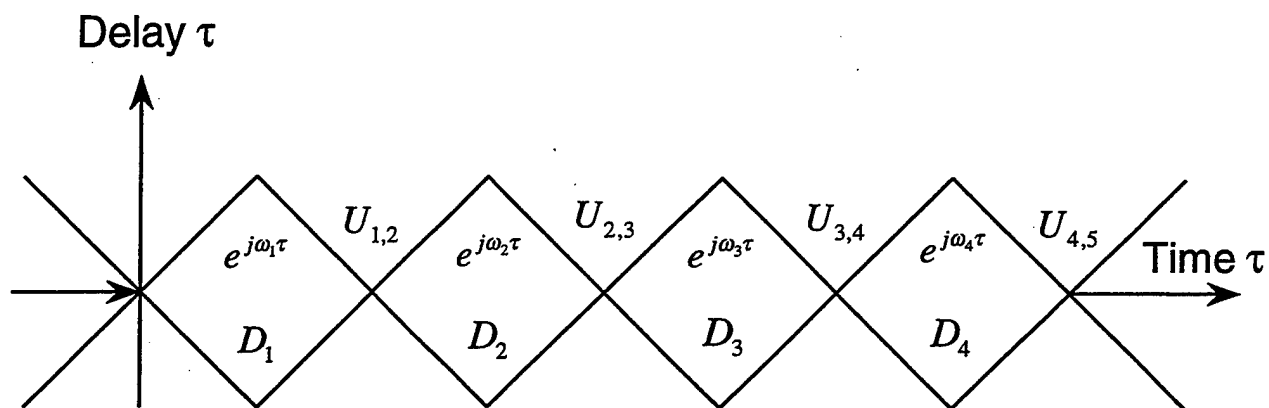
17

Figure 2a: Time behavior of an FH signal.

Figure 2b: FH signal and the cellular (diamond) structure of the ICF.

L^{th} hop, is given by: $\quad R(t,\tau) = e^{j\omega\tau}$,

where ω is the radian frequency of the complex valued sinusoid. We note that the values of

$(t+\tau/2)$ and $(t-\tau/2)$ are confined to be within the same L^{th} hop if they satisfy

$(L-1)T_h \leq (t+\tau/2)$ and $(t-\tau/2) \leq LT_h$. This inequality forms the boundaries of a diamond

pattern for a given value of L. This cellular structure is shown in Figure 2b. Inside each diamond

the ICF is obtained by correlating signals from the same hop, while outside the diamond the ICF

is obtained by correlating signals belonging to two consecutive hops.

The correlation function $R_{m,n}(t,\tau)$ (i.e., in region $U_{m,n}$) is given by:

$R_{m,n}(t,\tau) = \exp j (\omega_m - \omega_n) t + (\omega_m + \omega_n) \tau/2$; where m and n are the indices of the two adjacent

hops. We note that within the main diamond of the nth hop, (i.e., m=n), the ICF is given by

$R_{m,n}(t,\tau) = \exp j (\omega_n \tau)$ while outside the main diamond (i.e., in the upper triangle between hop

numbers n and n+1), the ICF is given by $R_{n+1,n}(t,\tau) = \exp \{j (\omega_{n+1} - \omega_n) t + (\omega_{n+1} + \omega_n) \tau/2\}$.

The lower half of the ICF has hermitian symmetry relative to the upper half and does not provide

any additional information.

In summary, the instantaneous correlation function of a FH signal will exhibit cellular

(i.e., diamond) patterns. Inside the Lth diamond the ICF has a single complex exponential

component along the delay axis representing the Lth hop frequency. Outside the diamond, $R^i(t,\tau)$

is a product of two terms, $\exp j (\omega_m - \omega_n) t$ and $\exp j (\omega_m + \omega_n) \tau/2$, where ω_m and ω_n are two

consecutive hop frequencies.

4. PROCESSING SCHEME

The wavelet transform generates one surface for each scale. One can visually inspect the wavelet surfaces to identify the FH signal and obtain an estimate for the hop time interval. Alternatively, one can use a processing scheme to estimate the hop start/stop times, the hop-scale pattern, and the hop frequency. For the extraction of the hop start/stop times an edge detector is used. An estimate of the hop-scale pattern can be obtained by performing an energy analysis.

The energy analysis assigns a scale index (called the proper scale) to each hop. The proper scale, is that scale which has the greatest energy content (i.e., spectral components live in the spectral region covered by the scale under consideration). The sequence of proper scales, representing the hop sequence, is called the hop-scale pattern.

If a hop-scale pattern is detected, it provides the evidence that a frequency hopped signal is present. If some or all frequencies of an FH signal reside in the spectral region of one scale then a follow-on spectral estimation will indicate different frequency components as a function of the hop intervals which still permits the identification of the FH process.

For FH signals, the ICF displays a cellular pattern (i.e., see Fig.2), where each hop results in a diamond pattern with a width equal to the hop interval. The diamond intersects the time axis at the hop start/stop times. The wavelet surface at the proper scale emphasizes signals which belong to that scale, while other signals (i.e., out of band components) are attenuated.

The interception problem usually assumes some prior knowledge about the signal of interest. In our case, we assume the minimum and maximum hopping frequencies are approximately known and the data is properly sampled.

4.1 Discrete-Time Implementation of the Instantaneous Correlation Function

Let $R(n,u)$ define the ICF of the discrete-time signal $x(n)$, given by:

$R(n,u) = x(n+u/2) x^*(n-u/2)$, where n is time and u is the delay. The combined index

$n \pm u/2$ should assume integer values. We can insert zeros into the ICF (i.e., $R(n,u)$, for odd u,

is set to zero), or we can let $u = 2m$. The last approach is the one adopted in this report.

A one-dimensional wavelet transform is performed in the direction of the delay u for

each time element of the correlation function. The Matlab wavelet toolbox [59] is used with the

convention that the highest band of passband frequencies is denoted by scale number 1.

4.2 VISUAL IDENTIFICATION

We investigated different types of wavelets as well as different surface representations. A

complex-valued Daubechies wavelet of order 3 is given in [60] and is used for comparison with

the real valued Daubechies wavelet of the same order. Operating on the complex valued ICF with

a real or complex valued wavelet results into a complex valued scale (surface) output. A complex

valued surface can be represented by its magnitude, phase or potentially the real or imaginary

component. A visual identification technique was used to select the type of wavelet and the type

of scale representation. Based on a large number of simulations in conjunction with an opinion

test it was concluded that a real valued wavelet will suffice and the surfaces, using the real

output, provide superior results. Hence in all follow-on work, real valued wavelets and real

valued scale surfaces are used. This processing approach was also verified using the Morlet

wavelet [56].

The objective of the opinion test is to identify the frequency hop, interpreting the cellular

structure in the wavelet surface, and to identify the diamond's time axis intercepts to serve as an

estimate of the hop start/stop times.

Figures 4.1 and 4.2 show examples of the real part of the WT obtained with the

real-valued Daubechies wavelet of order 3. Figure 4.1 and 4.2 display the real part of the IFC and

the real part of the first 5 scales of a FH signal with an SNR of 10 and 3 dB, respectively. The

frequencies of the FH signal are such that they hop the scales in a staircase fashion (i.e. time

segment 1 or hop 1 is on scale 1, time segment 2 or hop 2 is on scale 2, etc.). We note that we are

unable to identify the FH structure from the original ICF surface, denoted by "CF." Wavelet

surfaces, labeled "S1r", .., "S5r", allow identification of diamond patterns at hop number 1, .., 5

, respectively. The diamond patterns are detectable since they are presented by contour lines of

constant height that run from left to right. If we were to plot the delay trace that goes through a

diamond, for a given fixed value of time, we will observe a sinusoidal pattern having a fixed

frequency. These figures demonstrate that we can identify the FH structure from the wavelet

surfaces, while it is not possible to do so from the ICF surface. At high SNR's (i.e., 10 dB or

better), we can also determine the hop times (i.e., where the diamond intercepts the time axis)

easily. A color coded display is superior to the black and white representation used in this report.

4.3 ENERGY ANALYSIS AND SCALE IDENTIFICATION

If correct hop timing information is available, we can perform an energy analysis for each

hop. Parseval's theorem for the complete orthogonal filter bank (over L partitions) is applicable

to the discrete time wavelet analysis [45]. So $\|x(n)\|^2 = \Sigma_{a \in Z}$ ($|C(L,2a)|^2 + \Sigma_{j=1}^{L}$ $|d(j,2a+1)|^2$),

where C(L,2a) are the scaling coefficients at the scale L, d(j,2a+1) are the wavelet coefficients at

scale j, and a is the wavelet shift variable. The quantity $E(j) = \Sigma_{a=-\infty}^{\infty} |d(j,a)|^2$ represents the

signal energy over the jth scale. Energy per sample is defined as: A(j) = E(j)/ N(j), where j is the

scale index, E(j) is the total energy at the jth scale, and N(j) is the number of wavelet coefficients
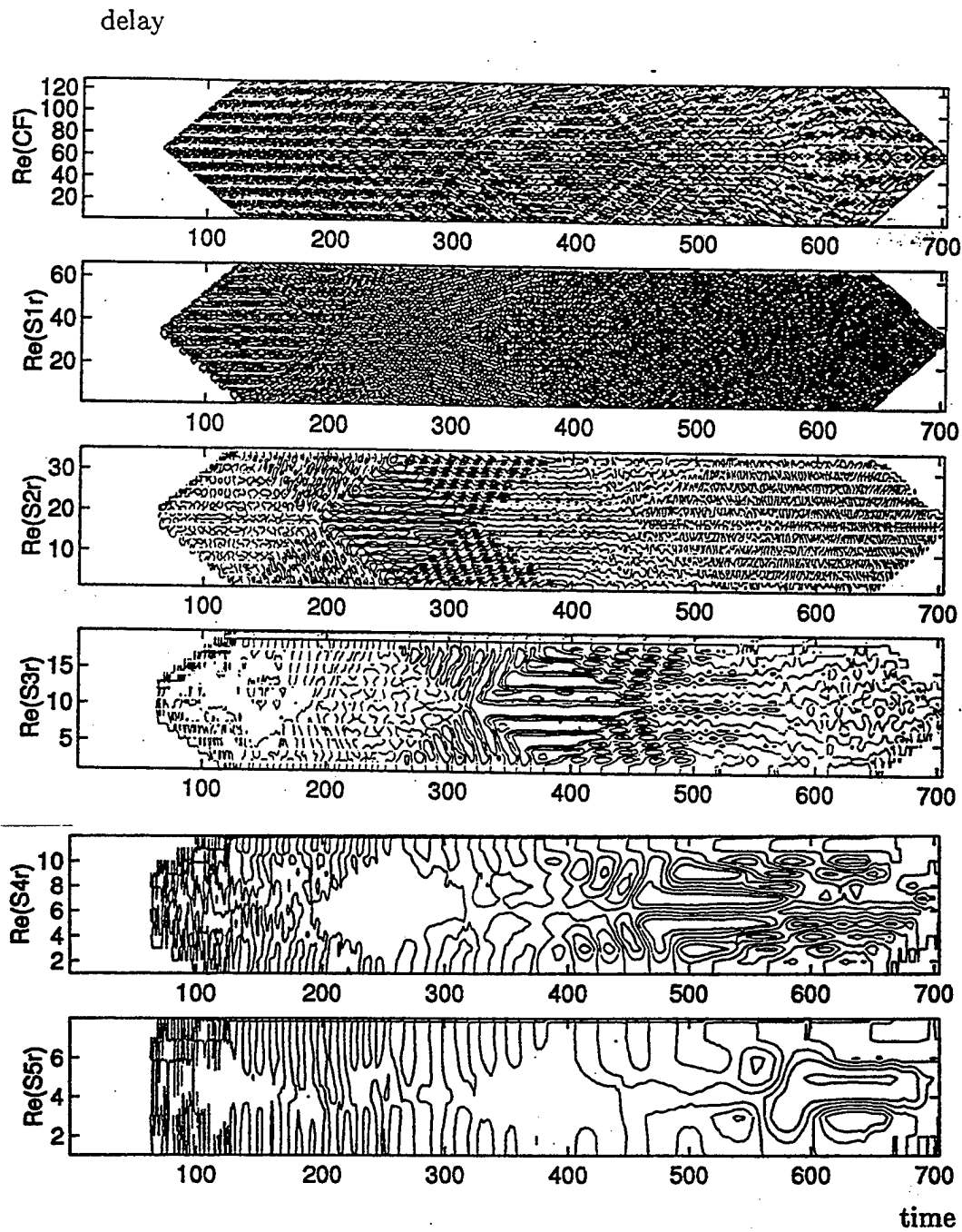
at this scale.

delay

Figure 4.1 Wavelet Surfaces of FH Signals Using Daub-3 at 10 dB (scale 1-5).
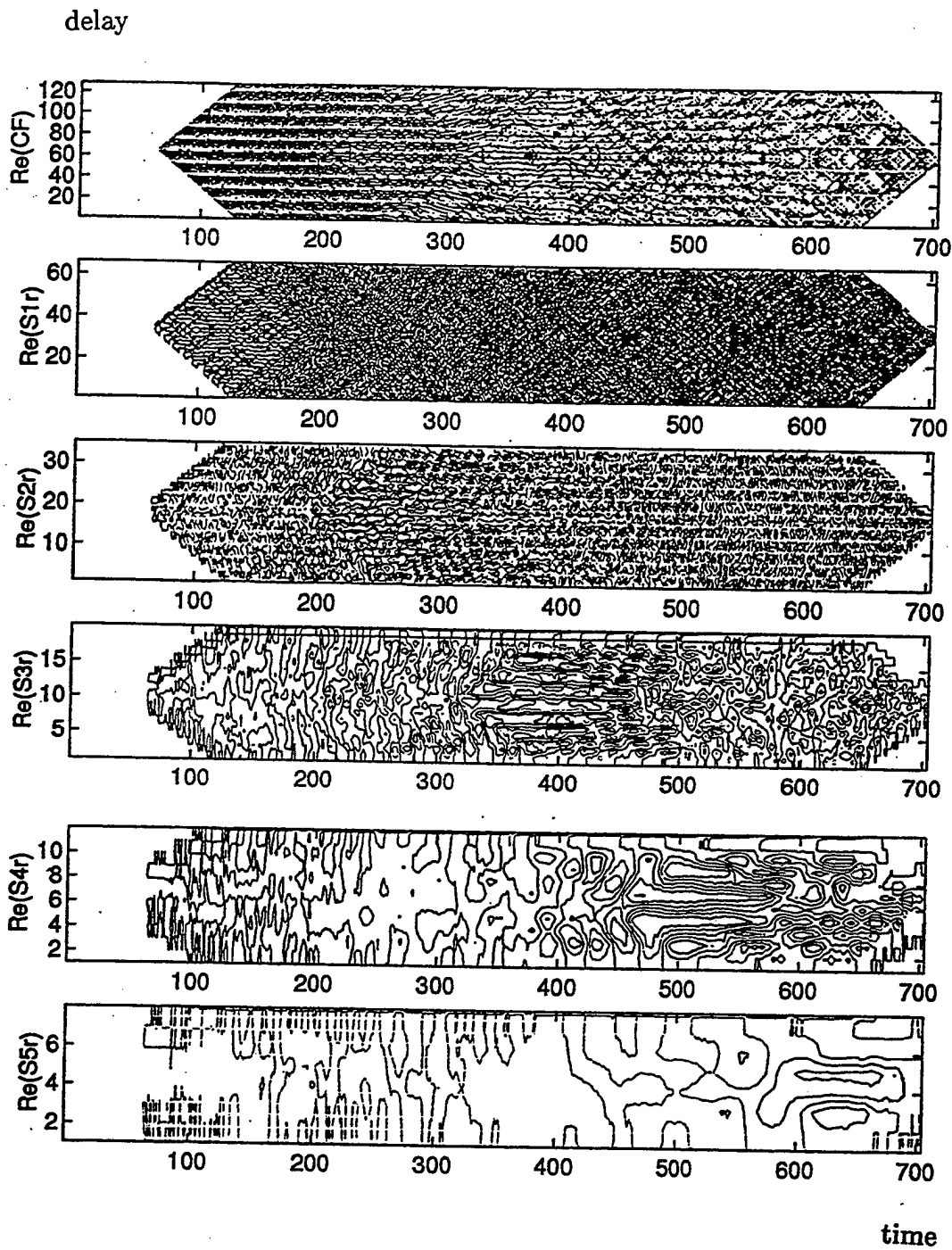
23

delay

Figure 4.2 Wavelet Surfaces of FH Signals Using Daub-3 at 3 dB (scale 1-5).

24

To identify the proper scale one can use the maximum value of the wavelet coefficients, the total energy, or the energy per sample. Table 1 summarizes the energy distribution obtained via wavelet analysis using Daubechies wavelet of order 2 (Daub-2) and order 10 (Daub-10). The signal is 64 samples long and consists of three sinusoids. The first signal has a frequency of 3/8 F_s, the second has 3/16 F_s, and the third has 3/32 F_s, where F_s is the sampling frequency. Hence the first, second, and third input signal is contained in the first, second, and third scale, respectively. Using the information from table 1 we can conclude that the total energy of the input signals is distributed across the scales and that the sum of the total energies over the scales is slightly less than the total signal energy since we disregard any contribution from the low pass section. The proper scale (where the signal resides) has the greatest share of the total energy. This share increases with an increase of the wavelet length. This is attributable to the smaller spectral leakage of longer wavelets. Energy per sample at the proper scale is larger if the signal resides at a higher scale. The gain factor in energy per sample (if the signal resides within scale 2 rather than scale 1) is about 1.41 and 1.64 for Daub-2 and Daub-10, respectively. Ideally, the gain factor in energy per sample should be 2 per scale index. For an automated detection scheme the energy or energy per sample is the superior test statistics. To declare that a signal belongs to a particular scale, that scale must be the dominant one relative to all other scales. The larger the ratio the better the discrimination. We note in table 1 that the energy and energy per sample outperform the maximum coefficient at all scales and all wavelet sizes tested.

4.31 Hop-Scale Pattern

The scale identification assigns a scale index to each hop of the observed signal. The hop is assigned to the scale whose energy per sample is the largest among the values of the other

Table 1: Energy Distribution of Daub-2 and Daub-10 Wavelets

Measure	Wavelet	Scale	Signal with $f = (3/8)F_s$	$f = (3/16)F_s$	$f = (3/32)F_s$
Max Coefficient	Daub-2	1	1.3365	0.6574	0.4349
		2	0.5753	1.6998	1.0356
		3	0.3743	0.3594	1.8480
	Daub-10	1	1.2524	0.3818	0.3284
		2	0.3968	2.0331	0.5504
		3	0.1854	0.3859	2.8296
Total Energy	Daub-2	1	29.7687	7.2565	0.8486
		2	1.1313	23.3282	8.2775
		3	1.0495	0.9492	21.2601
	Daub-10	1	31.4508	1.6228	0.4040
		2	0.3980	29.9017	1.9671
		3	0.0875	0.3900	29.0447
Sample Energy (average per sample)	Daub-2	1	0.9201	0.2199	0.0257
		2	0.0628	1.2960	0.4599
		3	0.1049	0.0949	2.1260
	Daub-10	1	0.7671	0.0396	0.0099
		2	0.0133	0.9967	0.0656
		3	0.0036	0.0163	1.2102

scales. This should correspond to the true scale location of the frequency hop and is called the proper scale. A sequence of hops will result in a sequence of proper scales forming the hop-scale pattern.

4.32 Success Rate

The performance of scale identification is evaluated via the success rate P_{id}. This is done by generating known hop-scale patterns and obtain the percentage of the correctly identified hop-scales. The success rate is defined as: P_{id} = number of correct hop-scales / total number of hops. The quality of scale identification depends on the height of the greatest energy per sample relative to the other sample energies from other scales.

The spectral density of the ICF for a white noise input, in the delay direction, has a triangular spectral shape. To allow comparison the spectral shape the energy per sample for all wavelet scales must be corrected accordingly. Performance in terms of the success rate P_{id} is given in chapter 5.

4.4 FREQUENCY ESTIMATION

The Fourier Transform of the wavelet surface gives a bandpass filtered version of the WVD. The hop frequency can be obtained from a Fourier transform over the delay direction of the wavelet surface (i.e., over the main diagonal of the appropriate diamond region).

The Fourier transform of the wavelet coefficients can be used as a spectral estimate (i.e., periodogram) at all scales. The frequency resolution dependents on the parameters of the Fourier transform.

The frequency resolution (i.e., the minimum spacing between two resolved narrow band

components) of the DFT is approximately equal to $\Delta f =/N$. At any given scale k, the number of data points N(k) is related to the number of input data points N by $N(k) = N/2^k$. The sampling frequency of the scale output (i.e., detail function) is scale dependent, i.e., $F_s(k) = F_s/2^k$, where F_s is the input sampling frequency. At the kth scale, both the number of data points (wavelet coefficients) and the sampling frequency have been reduced by the same factor. Consequently, the FT of the N(k) data points has a frequency resolution that is constant, independent of the wavelet scale being addressed.

4.41   Success Rate

Performance of the frequency estimation procedure is evaluated in terms of the success rate, P_f. The hop frequency is considered correctly estimated if the spectral peak is at the true spectral bin. P_f is defined as: P_f = number of correct hop frequencies / total number of hops.

The hop frequency is given by the bin number corresponding to the peak of the magnitude of the FT over a specified region of the wavelet surface. The quality of the frequency estimation depends on the spectral height of the peak relative to the average background.

Given the correct hop start/stop times, the hop frequency may also be estimated directly from the time signal or from the ICF surface. To extract the frequency from the original time signal we can use the FFT of the time data over the hop length. The FFT is a matched filter for sinusoidal signals in white Gaussian noise. Thus, an optimal performance is expected relative to the nonlinear processing of the signal through the ICF computation and the linear wavelet transformation.

We use P_{fc} and P_{fs} to denote the success rates of the frequency estimator when using the original time signal and the ICF surface, respectively. Results are provided in chapter 5.

28

4.5   ESTIMATION OF HOP TIMES

We recall that the ICF surface and wavelet surfaces have a cellular structure consisting of diamonds, where each diamond is associated with a specific hop. The diamond's interception of the time axis defines the start/stop point of the hops. The diamond width corresponds to the hop interval T_h. The sides (edges) of the diamonds of hops are mutually parallel and spaced by the hop interval T_h. There are many approaches one can use to solve the problem of hop time estimation. In what follows we will use a technique based on an edge detection operator.

Edge detection is a fundamental problem in image analysis since edges help in identifying objects. There are two basic types of edge operators, the gradient operators and the compass gradient operators [62,63]. The gradient operator measures the gradient of the two-dimensional image in two orthogonal directions. It is usually applied to detect edges with unknown directions. The compass operator measures the gradient of the two-dimensional image in a specific direction (i.e., $\pm \pi/4$ in the ICF or scale outputs).

The compass operator is applied to the upper half of the wavelet surfaces summing up all contributions according to the compass weights. The maximum value is extracted and determines the point where the compass array matches an edge. To make the data applicable to compass operations one needs to add a positive number, equal in magnitude, to the smallest (i.e., the most negative) surface value. Results are presented in chapter 5.

29

5. SIMULATIONS AND RESULTS

This chapter provides simulation results of the techniques introduced in chapter 4. Chapter 5 deals with wavelet transforms exclusively applied along the delay axis. We will address visual inspection, scale identification, frequency and hop time estimation. Results for wavelet processing along the delay axis are given in chapter 6.

5.1 VISUAL INSPECTION

To detect and to identify the FH modulation we performed an opinion test by examining the wavelet surfaces visually. Ten participants were involved, each one was asked to identify the diamond patterns of the FH signal from the wavelet surfaces at all pertinent scales and for all hops. Two types of wavelets were used; the Morlet wavelet and the Daubechies wavelet of order 3. Both wavelet types were used in their real and complex form. Four SNR values were used; 10, 6, 3 and 0 dB. Four different surface representations were examined; the real part, imaginary part, magnitude, and phase. To minimize biasing of the test results, all participants started to identify the surfaces going from the lowest SNR to the highest SNR value. More detailed scoring tables and the scoring code are given in [56]. The FH signal occupies the first five scales at different hop times.

Table 2 shows scoring results based on the real values of the scale surfaces for an SNR of 10 and 3 dB. 10 dB is the highest SNR value tested, while 3 dB is the minimum value that still provides an acceptable identification score. The values of the ratings range from 0.2 to 1. Here 1 indicates perfect identification of the hop diamond patterns at their proper time locations while 0.2 indicates just a detection of a hop pattern in the background noise.

The visual opinion test indicates that:

Table 2: Summary of the Identification Score Using the Real Part of the Scales.

Wavelet Type	SNR [dB]	Scales				
		S1	S2	S3	S4	S5
Real Morlet	10	1.0	1.0	1.0	0.95	0.95
	3	1.0	1.0	1.0	0.95	0.9
Complex Morlet	10	1.0	1.0	1.0	0.9	0.75
	3	0.7	0.8	0.9	0.5	0.4
Real Daub-3	10	1.0	1.0	0.8	0.2	0.2
	3	0.8	0.7	0.5	0.2	0.2
Complex Daub-3	10	1.0	1.0	1.0	0.3	0.2
	3	0.6	0.5	0.7	0.4	0.2

- Scores vary between 0.2 and 1, where

- 1 : perfect identification of hop diamonds.
    0.2: just distinction of hops from background noise.

i) The FH signal can be identified from the wavelet surfaces by its cellular structure which is dominant at the proper scales. That is, each scale will emphasize the hops which belong to the scale and attenuate other out of band spectral components. The (diamond) cellular structure can be used in the visual estimation of the hop start/stop times.

ii) The FH signal can be easily identified at SNR levels of -3 dB and above.

iii) The real part (or imaginary part) provides the best representation for visual inspection.

iv) The real value of the wavelet function provides a better surface representation than the complex valued wavelets. We tested the Morlet and Daubechies (Daub-3) wavelets [56]. Other types of wavelets may perform differently but were not evaluated.

v) Other modulation schemes such as ASK, PSK, MFSK and noise only patterns will have patterns residing at one scale only or have no discernible patterns at all. Typical plots are given in [56] verifying that if diamond patterns are noted at different scales, FH signals are present.

5.2 SCALE IDENTIFICATION

A processing scheme is used to extract hop start/stop times, the hop-scale pattern, and the hop frequency. Initially, we investigate scale identification and hop frequency estimation assuming that correct hop timing is available. Estimation of hop start/stop times is examined in section 5.4. For section 5.2 and 5.3 the parameters of the simulations are as follows:

i) Signal pattern length: 5 hops.

ii) Wavelet scales occupied: S1, S2, S3, and S4 (i.e., one scale is used twice).

iii) Wavelet types: Daub-2, Daub-4, and Daub-8.

iv) SNR range: -10 to 10 dB.

v) Number of realizations: 10 per scale per SNR value.

The hop frequencies of the FH signal are spaced to generate the hops according to a known fixed scale test pattern. The test pattern occupies scales S1 through S4. The wavelet surfaces are generated from the ICF surfaces at the relevant scales (i.e., scales 1 through 4). The total energy of each hop at each scale is computed and the energy per samples is obtained by dividing the total energy by the number of wavelet coefficients at each scale.

For each hop, the scale with the greatest energy per sample is designated as the proper scale. The resultant hop pattern is compared to the known hop pattern and the probability of correct identification is computed. To avoid bias from the colored noise of the ICF surfaces an equalization is performed at all scales prior to the estimation procedure.

Figures 5.1 to 5.3 show the performance of scale identification using the success rate P_{id}. Results are obtained for Daubechies wavelets of order 2, 4, and 8 for scales S1 through S4. For the scale identification performance we consider the minimum SNR at which P_{id} is still unity as the figure of merit. Over all tested scales the success rate, P_{id} assumes the value of 1 at different minimum input SNR values. This is a function of the order of the wavelet and the scale. Figure 5.1 shows that the performance of P_{id} obtained from Daub-2 achieves a P_{id} of 1 at an SNR of -1 dB at all scales, hence, -1 dB is considered the minimum SNR value for Daub-2. The minimum SNR value for Daub-4 is -2 dB at all scales as shown in Figures 5.2. Figure 5.3 indicates that an SNR level of -1dB or better is required to guarantee a P_{id} level of 1. For a P_{id} of 0.9 we need -1 dB, - 2 dB, and - 3 dB for Daub-2, Daub-4, and Daub-8, respectively. This shows that longer wavelets perform better than shorter ones in terms of Pid. The exception of that case is the performance at scale S1 to S4. The performance degradation, as the length of the wavelet is increased, may be due to a non-ideal equalization of the ICF spectral shape.
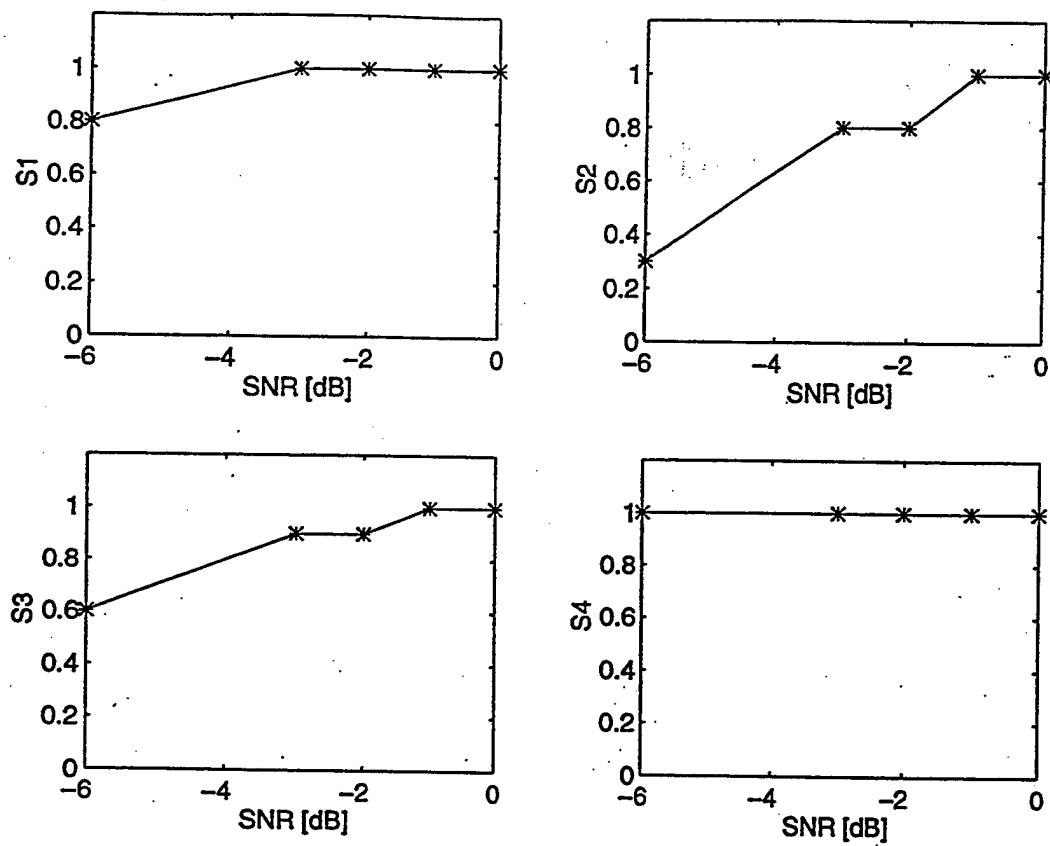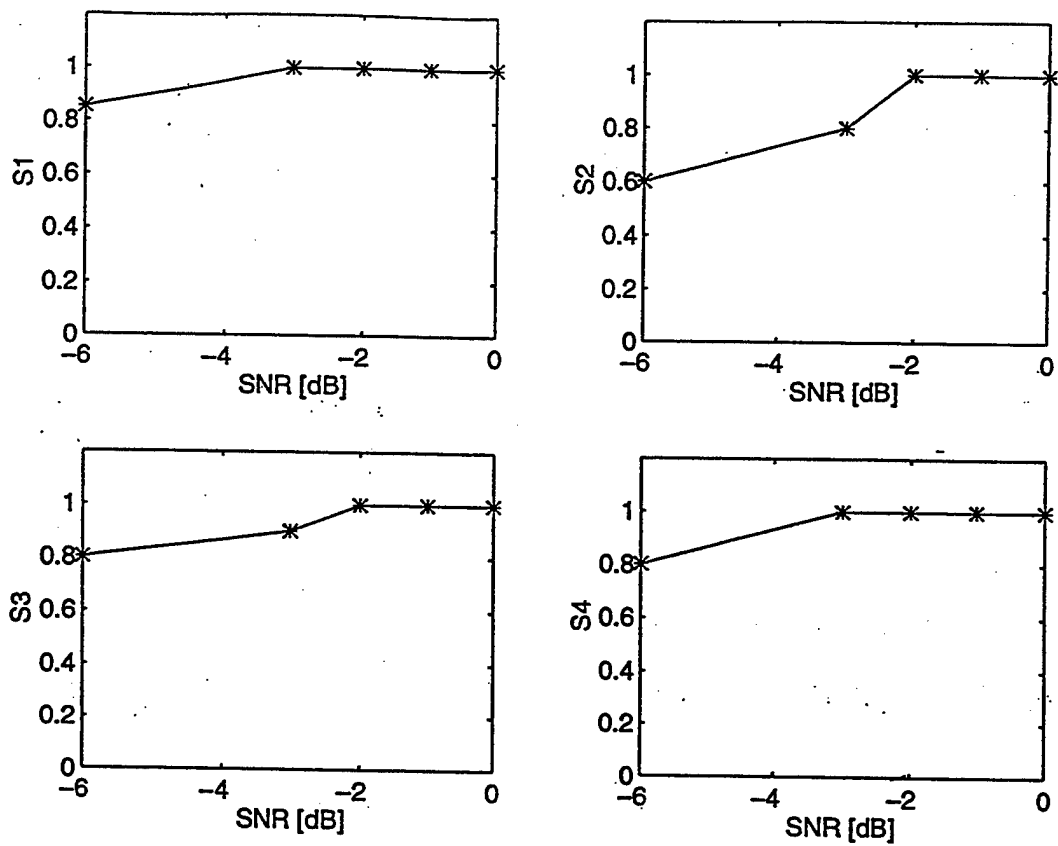
Figure 5.1 P_{id} for Daub-2.

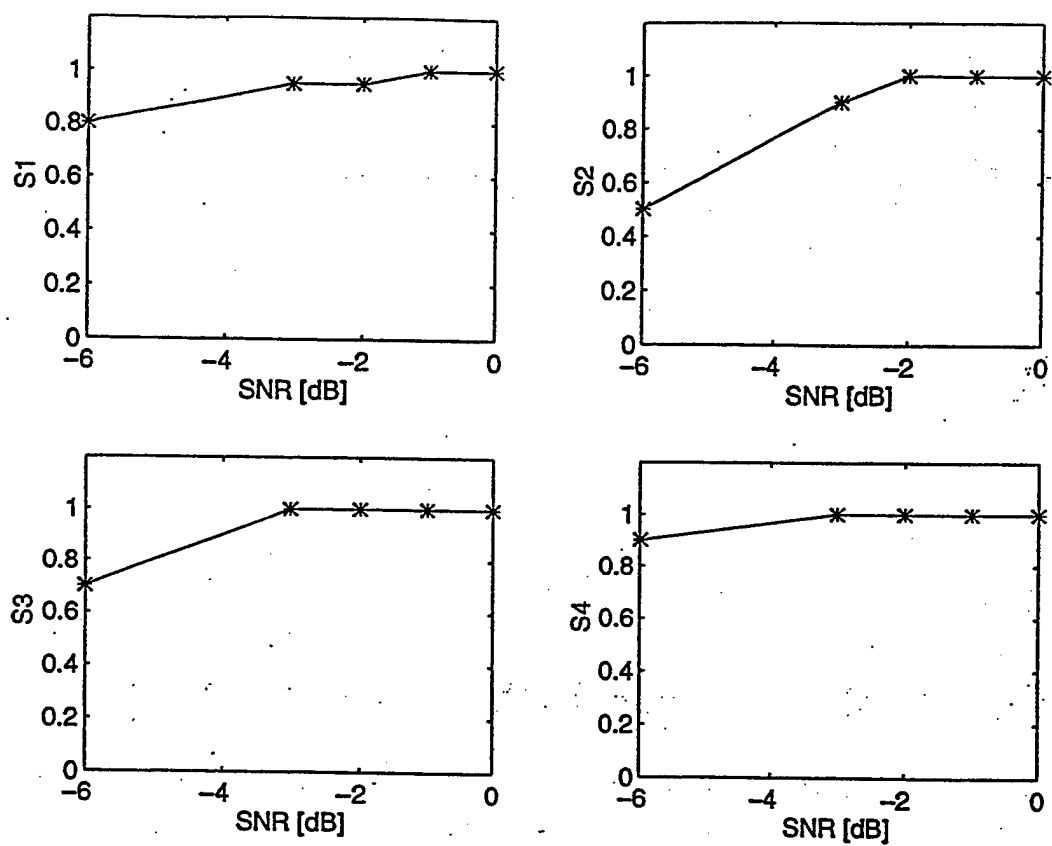Figure 5.2 P_{id} for Daub-4.

Figure 5.3 P_{id} for Daub-8.

Theoretically, wavelet surfaces at higher scales have higher SNR values than those at lower scales due to the reduced passband regions at higher scales. Generally, the scale identification performance increases with increases in scale number, wavelet length, and SNR. There are some small inconsistencies, but we attribute the anomalies to the non-ideal equalization and the non-ideal filter transfer functions (in a spectral sense).

5.3 FREQUENCY ESTIMATION

We carried out simulations to evaluate the performance of frequency estimation using the data specified in section 5.2. The hop frequencies are estimated by taking the FT of the wavelet coefficients located at the center of the diamond patterns in the direction of the delay. The bin corresponding to the peak value represents the estimated hop frequency. The estimated hop frequency is compared to the true hop frequency and the probability of correct frequency extraction (the success rate P_f) is computed. The estimated frequency is considered correct if the estimation error is less, in percentage of the true frequency, than 1/N, where N is the length of the vector of the wavelet coefficients. Figures 5.4 to 5.6 plot the success rate P_f obtained for different wavelets as a function of scale. For the frequency estimation we consider the minimum SNR for a given P_f value as the figure of merit.

Figure 5.4 shows that the P_f value for Daub-2 is 1 at an SNR equal to 0 dB at most of the scales. A P_f of 0.9 is obtained for all scales for SNR levels greater or equal to -1 dB. The minimum SNR value for Daub-4 and Daub-8 at a P_f of 0.9 is -2 dB, as shown in Figures 5.5 and 5.6. For Daub-2, Daub-4 and Daub-8 at a P_f of 1.0, the minimum SNR level is 0 dB at scales S1, S2, and S3.
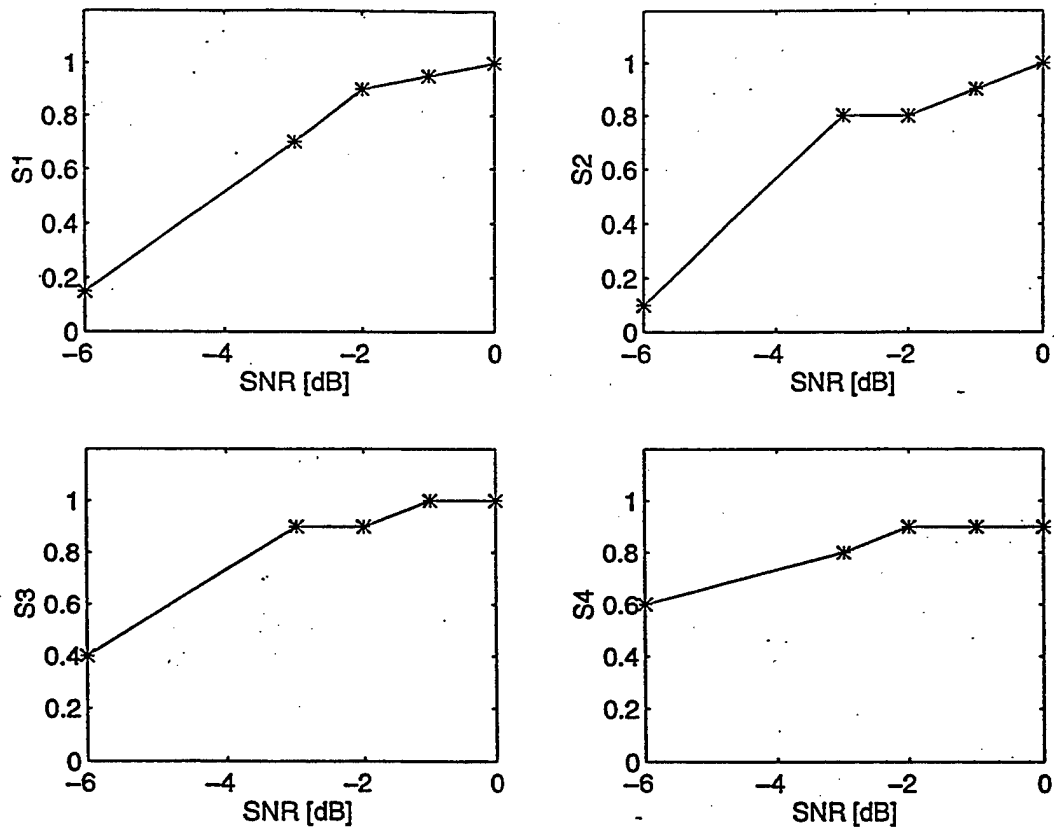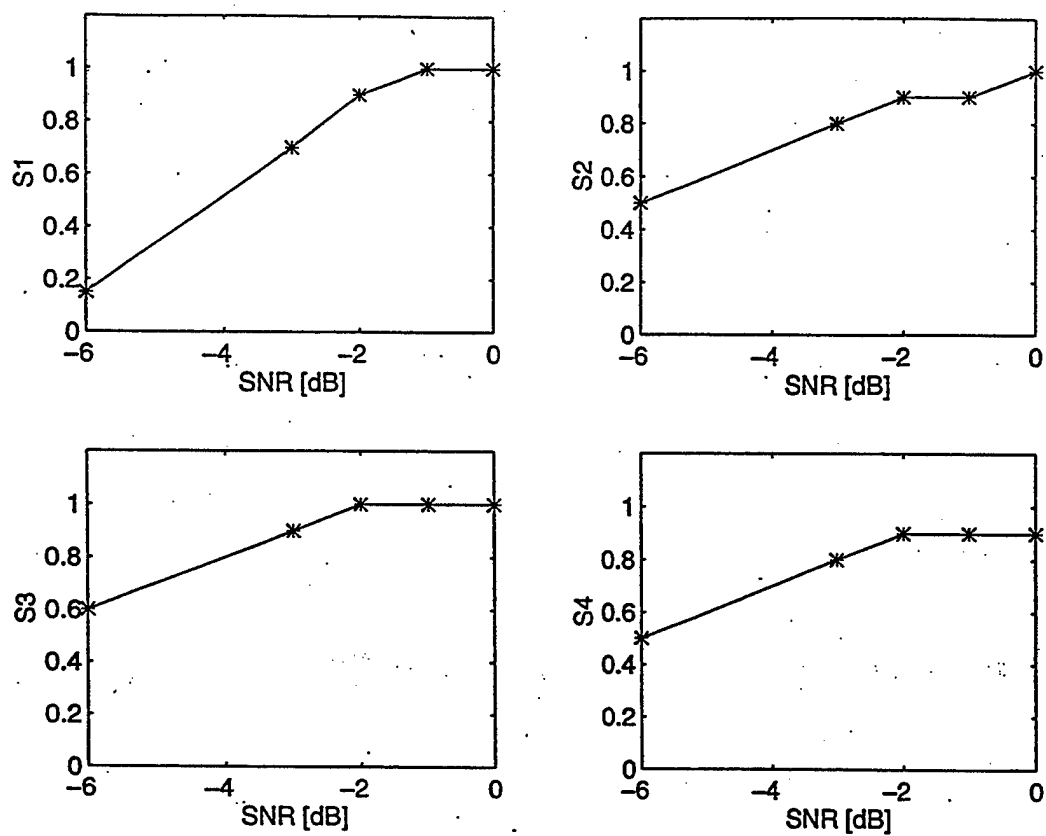
Figure 5.4 P_f for Daub-2.
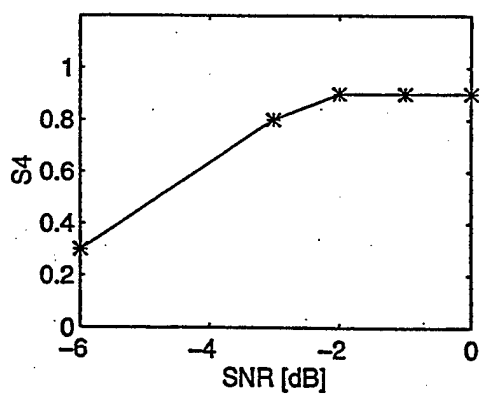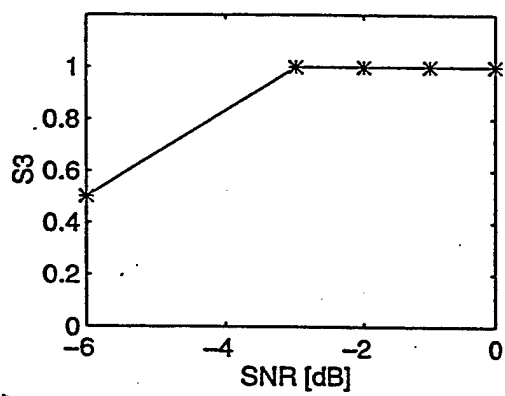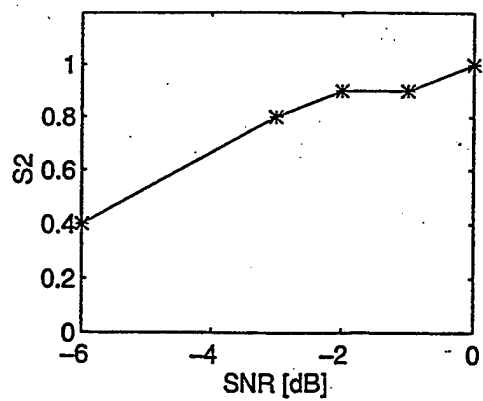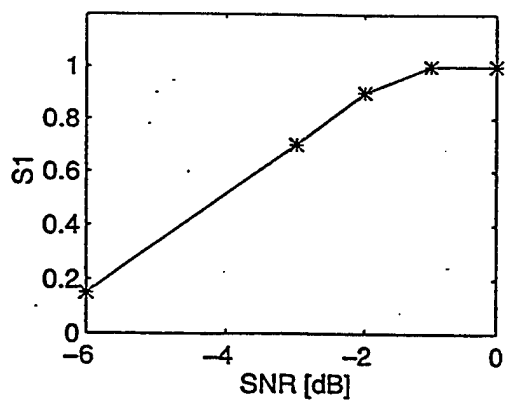
Figure 5.5 P_f for Daub-4.

Figure 5.6 P$_f$ for Daub-8.

Values of the success rate P_f show that the hop frequency can be reliably estimated from most wavelet surfaces at an SNR $\geq$ 0 dB by using only one FFT at the center of the diamond area in the direction of the delay.

Hopping frequencies may also be estimated directly from the original signal or from the ICF. Figure 5.7 plots the performance P_{fs} and P_{fc} obtained from the time signal and from the ICF, respectively. The plots are indexed by the SNR and assume that exact estimates of hopping start/stop times are available. By contrast, using the wavelet surface, under the best circumstances (i.e., scale 3, Daub-8), we need an SNR $\geq$ -3 dB to obtain perfect performance. The SNR should be about -3 to -5 dB for using the raw time signal (i.e., need hop timing information). The frequency estimation success rate using the ICF, at a P_{fc} of 1, requires an SNR value of 0 dB or better.

This shows that, assuming exact estimates of hopping start/stop times are available, hop frequencies may be estimated by processing the original signal at lower SNR values than can be achieved using the wavelet or the ICF surfaces. The benefit obtained by analyzing the ICF surface by wavelet analysis is significant in case of unknown hop start/stop times. We also note that fewer computations are needed when we estimate the frequency from wavelet surfaces. This is due to applying only one FT per hop, using few coefficients (i.e., decimated wavelet output).
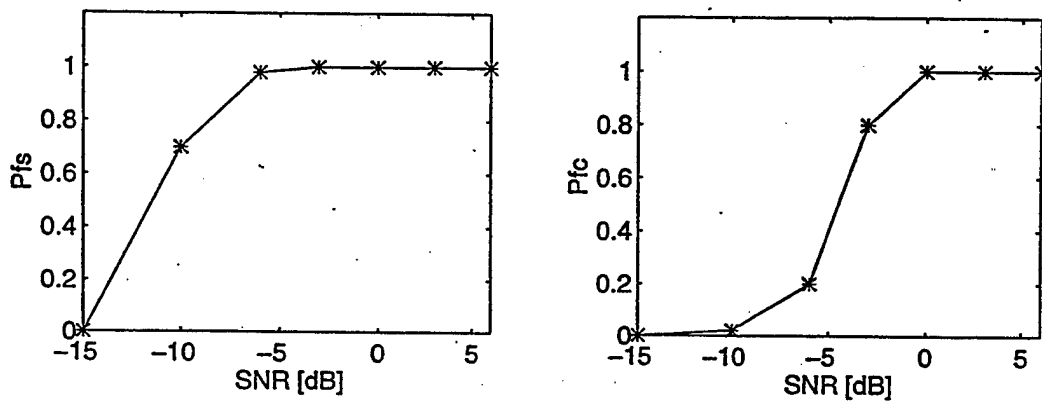
Figure 5.7 P_{fs} Using the Time-Signal and P_{fc} Using the ICF.

5.4   HOP TIMES ESTIMATION

This section presents hopping time estimation results obtained using the compass operator referred to earlier. The wavelet surface can be represented by its upper half plane. Then the areas of interest (i.e., Fig. 2) have a triangular pattern instead of a diamond pattern. The line compass operator is used over the surface moving from left to right. The location of the peak value of the resultant provides the hop start/stop time. The difference between the true and the estimated starting time is the estimation error. It is evaluated in terms of points of the time axis. For each SNR 20, realizations are used with a 128-point hop interval.

Figures 5.8a - 5.8c plots the mean square estimation error (MS) as a function of SNR and Daubechies wavelet length. At an SNR $\geq$ 10 dB, the MS is 200 or better. We notice that the shorter wavelet (i.e. Daub-2) has the better performance (i.e., at an SNR $\geq$ 6 dB the MSE is about 200). This observation agrees with the notion that longer wavelets relative to shorter ones have better frequency localization but have poorer time localization.
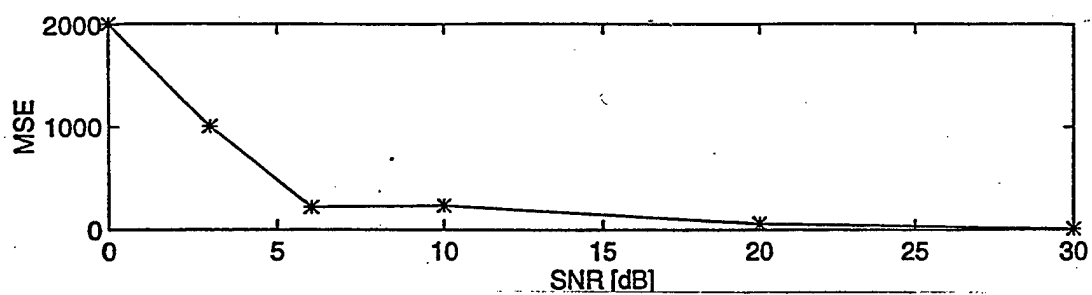
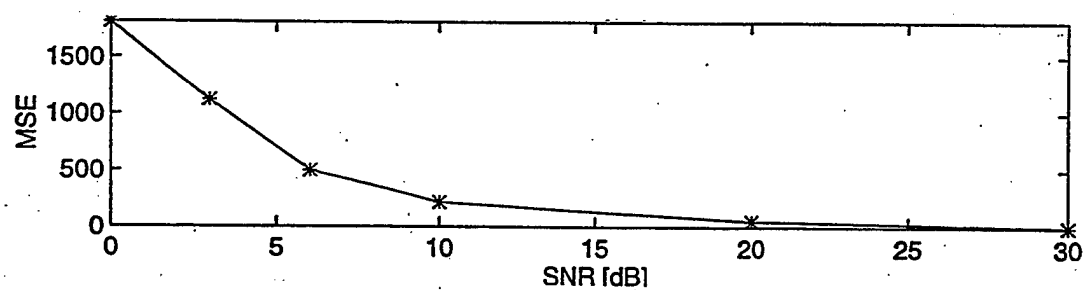Figure 5.8a Hop-Timing Mean Square Estimation Error for Daub-2.

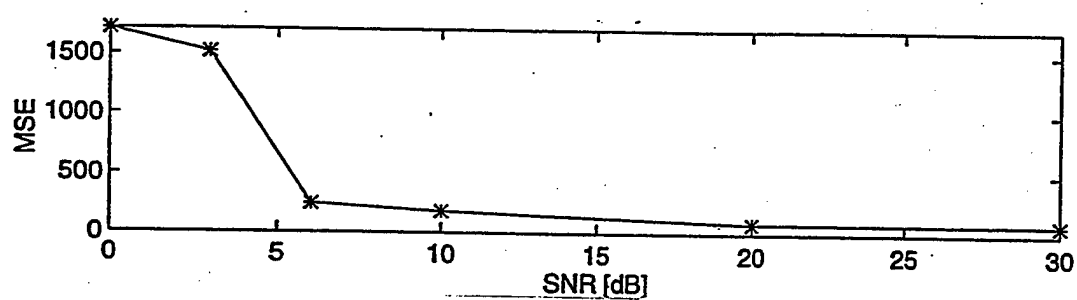Figure 5.8b Hop-Timing Mean Square Estimation Error for Daub-4.

Figure 5.8c Hop-Timing Mean Square Estimation Error for Daub-8.

6. Wavelet-Based Hopping Time Detection

6.1 INTRODUCTION

As discussed earlier, spread spectrum communications schemes have received ever increasing attention over the past two decades as numerous civilian applications have joined military applications [22,27,28,32,50,64]. Two main assumptions typically found in the literature are that the hop timing is constant and known, and that the hopping frequencies are selected from a known class of candidate frequencies. Even when the hop timing is not assumed known, it is still usually assumed constant [28]. These assumptions generally restrict the detection and estimation schemes to *frequency hopping* (FH), one of the more popular spread-spectrum communications techniques.

The primary goal of this section is to provide a new approach for the detection and estimation of frequency hopping signals which makes none of the restrictive assumptions listed above. By not making such restrictive assumptions, it is hoped that a secondary goal is obtained. This goal is the application to the detection and estimation of other spread-spectrum communications techniques, such as direct sequencing, time hopping and hybrids of the three.

Section 6.2 briefly reviews the definition of the temporal correlation function used as the backbone of the analyzing scheme. Section 6.3 introduces the preprocessing tools used to increase the robustness of the analyzing to noise. Next, Section 6.4 briefly explains how wavelet analysis fits in our procedure. Section 6.5 presents the detection scheme developed. Section 6.6 presents the overall detection algorithm and simulation results. Finally, Section 6.7 provides conclusions and proposed extensions.

6.2 TEMPORAL CORRELATION FUNCTION

The *temporal correlation function* (TCF), also called ICF, of a signal $x(k)$ is defined as:

$$TCF_x(k,\tau)=x(k+\tau)x^*(k-\tau),$$

where k is the absolute center time and τ is the lag time, expressed in number of samples. Consider the following analytical frequency hopping signal x(k) given by:

$$x(k)=e^{2\pi j f_1 k}\left[u(k)-u(k-T_{hop})\right]+e^{2\pi j f_2 k}\left[u(k-T_{hop}+1)-u(k-T)\right],$$

for $0<k<T$, where T_{hop} is the time of the hop (or change in frequency) from f_1 to f_2, and where $u(k)$ is the unit step function. The resulting TCF function is defined as:

$$TCF(k,\tau)=e^{2\pi j(2f_1)\tau}D_1(k,\tau)+e^{2\pi j(2f_2)\tau}D_2(k,\tau)+e^{j2\pi[(f_2-f_1)k+(f_1+f_2)\tau]}D_{12}(k,\tau)$$
$$=TCF_1(k,\tau)+TCF_2(k,\tau)+TCF_{12}(k,\tau),$$

where $TCF_1(k,\tau)$, $TCF_2(k,\tau)$, and $TCF_{12}(k,\tau)$ represent the 1st, 2nd, and 3rd non overlapping terms contained in the TCF expression. Note that computing the TCF of the real frequency hopping signal has drawbacks as additional "crossterms" are present in the resulting expression, making the frequency identification process more complex [63]. Thus, we only consider the analytical frequency hopping signal. In practical situations, the analytical signal can easily be generated by applying a Hilbert transform to the real signal [50].

Figure 6.1a presents the phase plot of an analytical frequency hopping signal x(k) for some arbitrary f_1 and f_2, hoping time T_{hop}=208, and for positive τ values. The combinations of the different shifted versions of the unit step functions force the TCF to take on non-zero values only within the overall triangular within the regions shown in Figure 6.1a. Note that:

1) $TCF_1(k,\tau)$ is a function of f_1 and τ only. The second term, $TCF_2(k,\tau)$, is a function of f_2 and τ only, while the last term, $TCF_{12}(k,\tau)$, is a function of f_1, f_2, k, and τ.

2) The frequency hopping time T_{hop} is located where the region covered by $TCF_1(k,\tau)$ ends and the region covered by $TCF_2(k,\tau)$ begins.

3) For a given value of τ, the terms within the triangular regions (i.e., the regions where $TCF_1(k,\tau)$ and $TCF_2(k,\tau)$ are defined) are constant, although at different levels, while the phase behavior within the "cross-terms" region, $TCF_{12}(k,\tau)$ is linear. This fact is further illustrated in Figure 6.1b which plots the unwrapped phase of the TCF function for the value τ=30. It is important to realize, however, that the phase values over these three regions are a function of f_1 and f_2 and, therefore, not predictable without knowing f_1 and f_2, which in general we do not. Nevertheless, for any given value of the lag, $\tau < T_{hop}$, this region of cross-terms is centered on the hop time, T_{hop}, another fact which is exploited.

6.3 PREPROCESSING STEPS

The main idea behind the proposed scheme is to take advantage of the TCF phase behavior along the time axis k (i.e., for fixed values of τ). As shown earlier the unwrapped TCF phase along the time axis is constant prior and after the frequency jump, while it is linear in a region centered around the frequency hopping time, resulting in a constant-ramp-constant phase behavior along the time axis k, as illustrated in Figure 6.1b. Differentiating such phase leads to a pulse centered around

47

the hopping time, as shown in Figure 6.1c. Detecting the edges of the pulse is then all what is needed to identify the hopping time, as it can then be estimated as the midpoint between the two edges. Therefore, the hopping time detection problem can be viewed as an edge detection problem, which the wavelet transform is well-matched to address.

However the additive noise contained in the communication signal results in phase noise, degrading the quality of the resulting pulse. Furthermore, the differentiating step increases the effects due to noise. Thus, we apply median filtering before and after the differentiating step to minimize these phase noise effects. The main advantage behind this filter is that it preserves the ramp and step behavior and eliminates outliers. The length of the median filter operation was selected in order to preserve the step discontinuities present in TCF(k,τ) for fixed τ. Further details may be found in Overdyk [63].

6.4 WAVELET TRANSFORM BASED DETECTION

Edge detection is an important problem in numerous applications ranging from image processing to transient detection, and wavelet transforms have been used extensively for detecting discontinuities in a given signal or its derivatives. Recall that wavelets may be used to detect discontinuities in a signal or its derivatives, if the chosen wavelet function is able to represent the highest order derivative present in the signal function, as any wavelet with, at least p vanishing moments, can be used to detect a discontinuity in the (p-1)st derivative [46]. For our problem, we are interested in identifying pulse edges, i.e., a signal discontinuity, and the Haar wavelet is sufficient for the task. In addition, detecting discontinuities can be done quite simply using the decimated version of the wavelet transform [46].

The presence of noise makes identification of discontinuities more complicated. In such a

case, the averaging of several scales can enhance the wavelet's ability to detect discontinuities in noise. The basic idea is that for true discontinuities, the spikes will line up, while those associated to noise will not [46]. As a result, we averaged the first two scales in our simulation to improve the robustness of the detection scheme to noise degradations.

Figure 6.2a plots the result obtained by averaging the first two scales of the DWT applied to the unwrapped phase of the TCF expression for an analytical frequency hopping (FH) signal. The FH function has frequencies on either side of the hop, located at time sample 208, f_1 = 6.250 MHZ and f_2 = 22.727 MHZ. The SNR level is equal to 10 dB. Figure 6.2b illustrates the resulting wavelet transform of the pre processed phase of the TCF obtained at lag τ=30. Figure 6.2b shows that the wavelet transform clearly detect the location of the pulse ends, as expected. Note that the width between each spike obtained from taking the wavelet transform of the TCF phase along the time axis k (i.e., for fixed lag time τ) increases as τ increases. The next step sums all the values which represent the edges of the cross-terms in the TCF in 45° and 135°directions so that they reinforce each other, as illustrated in Figure 6.3b. Figure 6.3c shows the "detection vector" obtained from this summation. Further details may be found in Overdyk [63]. Note that the resulting spike is located at the hopping time T_{hop}=208.

6.5   DETECTION SCHEME

Once the detection vector has been formed, a decision must be made as to whether or not a hop has occurred within the frame. Experiments suggested that the variance of the detection vector would be the best indicator of whether or not a hop had occurred. As a result, the threshold, $T_{threshold}$, is chosen as a multiple, k, of the variance of the detection vector when no hop has occurred within

49

the frame. The threshold determination was also guided by the fact that the cost associated with the probability of a missed detection, $P_m = [1 - $ probability of detection $(P_D)]$ far outweighs the cost associated with the probability of a false alarm, P_{FA}, as the hopping time estimation is only the first step in a complete frequency hopping signal detection scheme. This is described in detail in the next paragraph.

Note that once the hopping times are estimated, the signal frequencies need to be extracted to demodulate the actual message. This step can easily be done by applying frequency analysis to the estimated hopping intervals. Thus, in the case of false alarms, frequency analysis would show the same frequencies in two, or more, consecutive hopping intervals, resulting in no message degradation. However, a missed hopping time will result in degradations in the frequency estimation step, and errors in the decoded message. Receiver operating characteristics (ROC) curves were generated for six SNR levels and an appropriate threshold chosen for each. Further details regarding the choice of specific thresholds may be found in Overdyk [63].

6.6 DETECTION ALGORITHM AND RESULTS

As stated earlier, it was desired to make as few assumptions as possible on the nature of the frequency hopping signal. With this goal mind the assumptions were limited to three:

1. Known spread spectrum frequency range. This range was assumed to be limited from 1 MHZ to 24 MHZ in the simulations conducted,

2. Known minimum hopping time, T_{hop_min}. This parameter was chosen to be equal to 256 sample points in our simulations. At a sampling rate of 50 MHZ, this translates into a minimum hopping time of 5.12 µs,

3. Minimum frequency differential, Δf, for frequency hops. This parameter was chosen to

50

be 1 Khz in our simulations.

Detection Algorithm

Using the tools described above, the algorithm steps for the detection and estimation of frequency hopping signals in noise can now be enumerated as follows:

1. Transform the real signal into an analytic signal.

2. Segment data into frames of length less than or equal to the minimum hopping time, T_{hop_min}. This assumption ensures that, at most, one hop will be present in the processing frame.

3. Compute the *temporal correlation function* on each frame.

4. Extract the TCF phase information and unwrap the phase along the time axis k.

5. Apply a median filter to the phase of the TCF along the time axis k, of length 5. This step is done to reduce the noise effects prior to differentiating, since differentiating accentuates the effects due to noise.

6. Differentiate the phase information along the time axis k. This step changes the unwrapped phase of the TCF from a ramp function to a pseudo-pulse.

7. Apply a second median filter along the time axis k of length 25. The length of 25 has proven to work well with the T_{hop_min} chosen for our simulations [63]. This step is done to again remove the effects due to noise which were accentuated by the differentiation operation in step 6.

8. Calculate DWTs along the time axis k (i.e., for each lag, τ, of the TCF) using the Haar wavelet. This step is done to detect the discontinuities at the edges of the cross-terms region.

9. Average the wavelet coefficients of the first two scales of the DWT.

10. Perform a 45°/135° summation across all values of lag, τ, to obtain a detection vector which has time as its index.

11. Threshold the data in the resulting detection vector obtained in step 10. When detected above the threshold, the maximum peak value time index represents the estimated hopping time.

Simulation results

Simulations were conducted to test the effectiveness of the detection and estimation algorithm given above. Five hundred trial experiments were conducted in six different signal to noise ratios (SNR) between -3 to 15 dB. The basic idea behind the experiments was to simulate signals that had already been segmented, as specified in steps 1 and 2 of the algorithm. The problem then becomes to determine: a) whether or not a frequency hop exists within the given frame; b) to estimate the hopping time when a frequency hop is detected.

Communication signals were generated by choosing random hopping time, T_{hop}, and hopping frequencies f_1, f_2 selected randomly in a predefined range. The resulting signal is a signal with, at most, one hop which can be from any frequency, f_1, to any hopping frequency, such that 1 MHZ $\leq$ $f_1, f_2 \leq$ 24 MHZ.

Table 6.1 shows the probability of detection, P_D, the probability of false alarm, P_{FA}, and the percentage of errors in classification for the selected threshold, $T_{threshold}$, at each of the six SNRs considered. Note the entries under the column labeled "k" represents a multiple of the variance of the detection vector generated from a "no hop" frame for each respective SNR level. The column

52

labeled "% Error" shows the percentage of mis classifications (i.e., the percentage of false alarms plus misses). Note, also, that the low probability of false alarm was sacrificed for higher probabilities of detection for reasons discussed earlier. For example, the entries in the row for SNR = 3 dB show that if a 11.4 % mis classification rate and a P_{FA}=0.1961 can be tolerated, then we can expect to detect 89.53% of the hops in a given frequency hopping signal.

Simulation results are shown in Table 6.2. The column labeled "Avg. Error" gives the average error obtained at each SNR level. For example, at the SNR level of 3 dB, out of all the hops which were detected, the average distance from the true hopping time was 10.48 sample points (i.e., 4.1% of the minimum hopping time). Columns with numeric headings indicate the hop detection probability within a given percentage of T_{hop_min}. For example, at the SNR level of 3 dB, the column labeled "1%" indicates that 36% of all *detected* hops were located within 1% of T_{hop_min} or within 2 points of the true hop time, T_{hop}. Similarly, 72% of all detected hops were located within 5% of T_{hop_min} or within 12 points of the true hop time, T_{hop}.

6.7 CONCLUSIONS

This section considered the application of temporal correlation functions and wavelet analysis to the detection and estimation of frequency hopping signals in additive white Gaussian noise. The algorithm developed has only two restrictive assumptions: 1) a minimum hopping time; 2) a minimum frequency differential. Thus, it can find applications where the minimum hopping time is not held constant; i.e., in *time hopping* signals and hybrid techniques involving either *frequency hopping* or *time hopping*. We showed how the detection problem can be formulated as an edge detection problem, and how wavelet analysis can be used in the hopping time detection problem.

Third, we introduced preprocessing techniques designed to improve the robustness of the detection and estimation scheme in noisy environments. Results show that the scheme is robust to noise degradations down to 3 dB.

Although the algorithm developed succeeded in meeting its goals, improvements can potentially be obtained by taking advantages of the specific two-dimensional structure of the hopping pattern. Thus, a possible extension involves considering the problem as an image processing or pattern recognition problem, due to the specific triangular pattern generated by the TCF of frequency hopping signals. As a result, applying more sophisticated two-dimensional edge detection schemes may improve the robustness of the detection and estimation scheme to noise distortions. As in the first part (i.e., chapters 1-5), improvements in the estimation of the TCF (or ICF) will improve the performance of the estimation procedure, that is improve detection and estimation of hop times. Such extensions are left for further research.
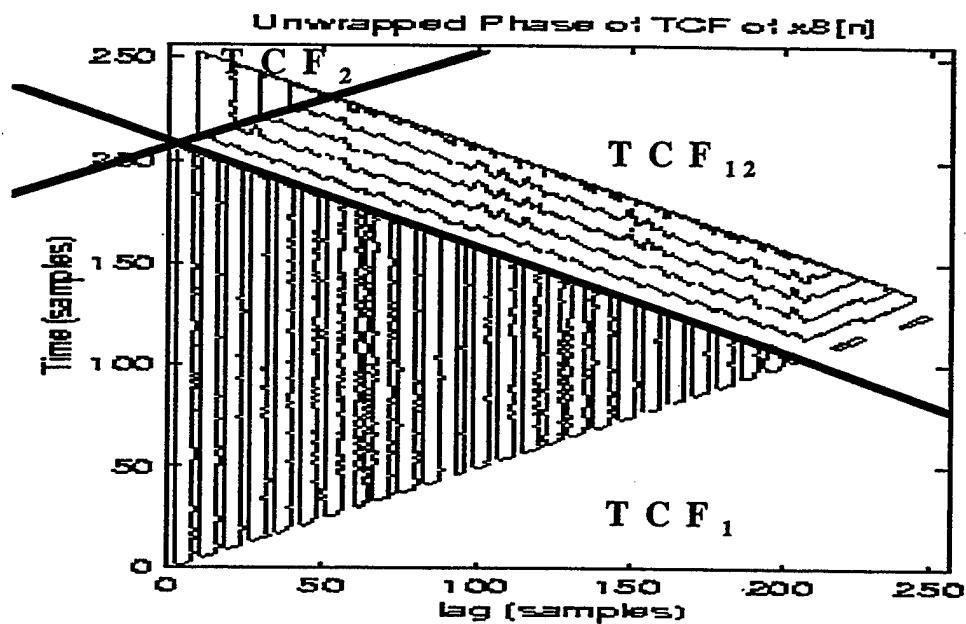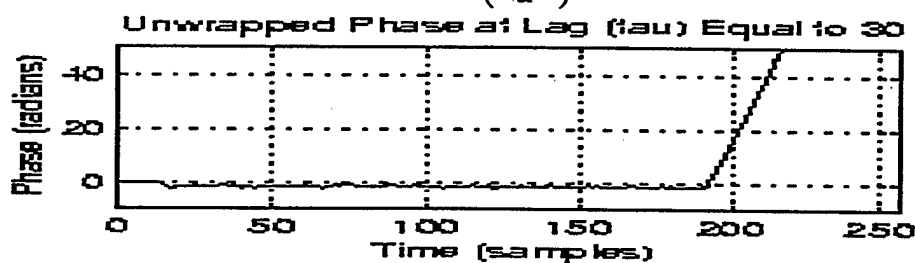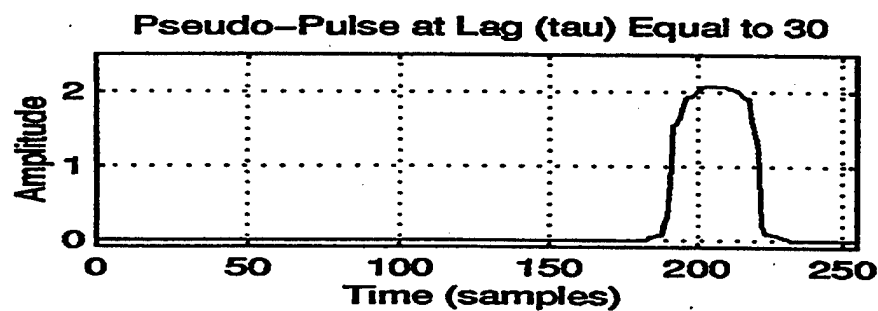
Figure 6.1: The unwrapped phase information of (a) the TCF, (b) for τ=30, and (c) after differentiating and median filtering for τ=30.

DWT on Preprocessed TCF of x8[n]

DWT on Preprocessed TCF at Lag 30

(a)

(b)
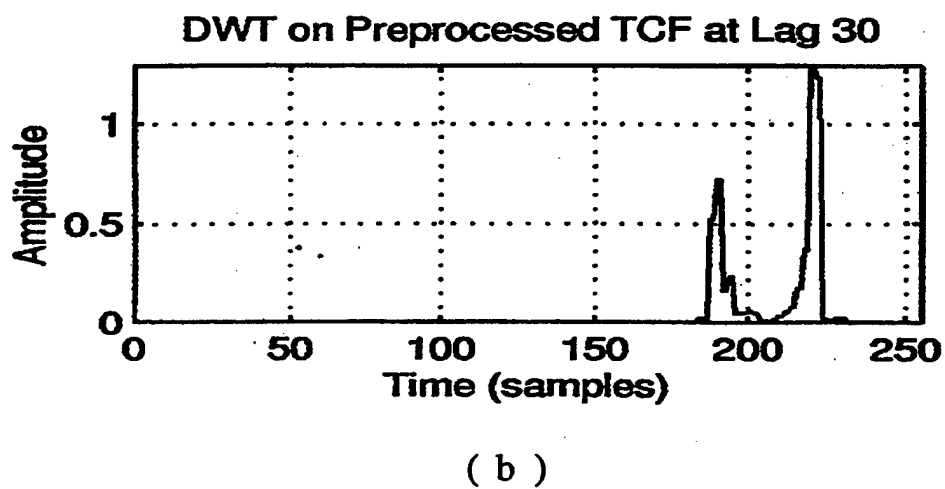
Figure 6.2: DWT coefficients computed for each value of lag τ (a) on the preprocessed phase of the TCF(t,τ), and for τ=30.

Figure 6.3: Detection vector constructed by performing a 45°/135° summation. (a) shows effects of the summation in (b) where the arrows indicate the direction of summation. (c) shows a plot of the actual detection vector.

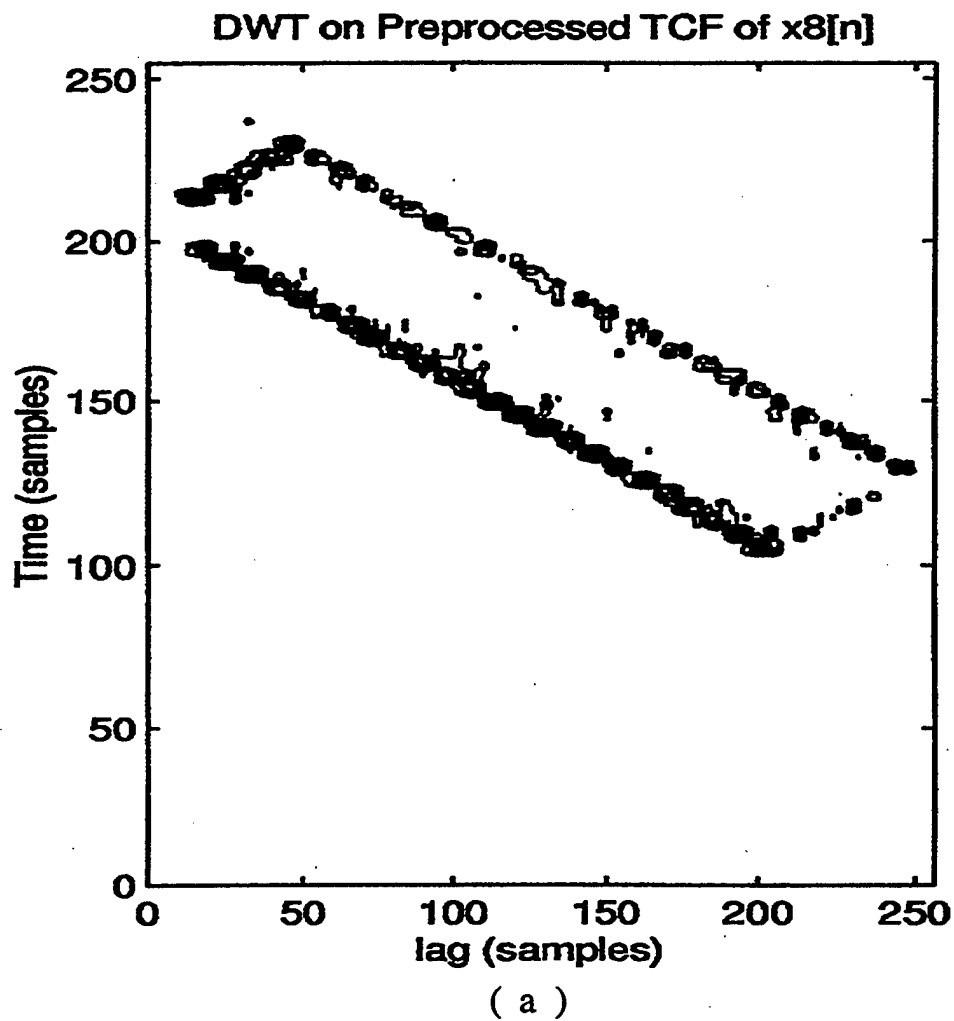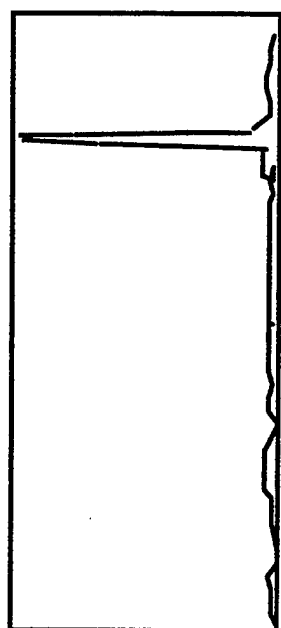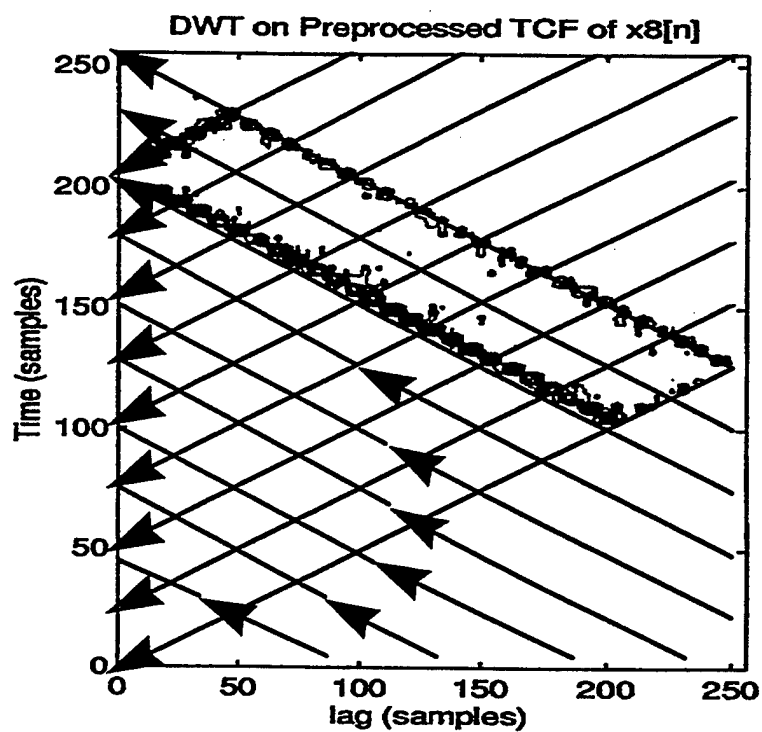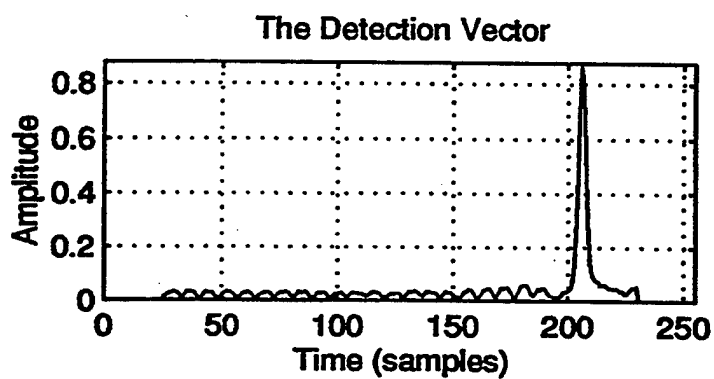| SNR	k	P_d	P_{fa}	% Error
15 dB	140	1	0	0.0
10 dB	30	0.9866	0.0196	1.4
6 dB	15	0.9844	0.1569	3.0
3 dB	11	0.8953	0.1961	11.4
0 dB	1	0.8129	0.3529	20.4
-3 dB	3	0.6927	0.3333	31.0

Table 6.1: Detection statistics of 500 experiments applying the detection and estimation algorithm.

SNR (dB)	1%	5%	10%	15%	20%	30%	40%	50%	75%	100%	Avg. Error (# of samples)
15	0.790	0.984	0.992	0.996	0.996	0.998	1.00	1.00	1.00	1.00	2.22
10	0.726	0.964	0.974	0.978	0.982	0.986	0.986	0.986	0.986	0.986	2.70
6	0.558	0.888	0.926	0.940	0.950	0.960	0.968	0.970	0.970	0.970	5.46
3	0.360	0.720	0.758	0.794	0.828	0.862	0.874	0.882	0.886	0.886	10.48
0	0.116	0.302	0.418	0.510	0.572	0.684	0.752	0.768	0.796	0.796	28.48
-3	0.090	0.174	0.276	0.382	0.456	0.568	0.614	0.646	0.686	0.690	30.99

Table 6.2: Estimation statistics for the 500 experiments at each SNR level using the detection and estimation algorithm described in Section B. Columns with numeric headings, show the probability that estimated hops are found within a given distance, expressed in percentage of T_{hop_min}, from true hopping times.

7. CONCLUSIONS AND RECOMMENDATIONS

7.1 CONCLUSIONS

Wavelet analysis of 2-D correlation functions is a new area of investigation. It can be applied to the interception of communication signals. This work aims at applying wavelet analysis to the instantaneous correlation function to identify frequency hopped signals. The instantaneous correlation function (ICF) of the complex-valued FH signal is shown to have a cellular (diamond) pattern, where each hop generates one main diamond structure. Inside a given diamond, the ICF of the signal consists a single complex exponential component representing the hop frequency in the delay direction and some noise. In the time direction, inside a given diamond pattern, the wavelet transformed data tends to be a constant perturbed by noise. The intersections of the diamond with the time axis determine the hop start/stop times while the width of a given diamond corresponds to the hop interval.

The wavelet transform of the ICF surface generates a number of surfaces. The wavelet surface, at any scale, emphasizes the frequency hops which reside there and attenuates spectral components that do not belong to the particular scale (i.e., bandpass filter) under consideration.

If we apply the wavelet transform along the delay axis, we can address the interception problem in two different ways. We can visually inspect the wavelet surfaces to identify and classify based on the structure the modulation due to an FH signal. This also allows to obtain a rough estimate of the hop time interval. Alternatively, we can apply a processing scheme which can be used to automate the interception task. This processing scheme estimates the hop start/stop times, the hop-scale pattern, and the hop frequency.

The estimation of the hop start/stop times can be addressed using an edge detection approach. We applied a compass operator to find edges in the wavelet filtered ICS. The hop scale

pattern is obtained by applying an energy analysis.

The frequency of each hop can be extracted from the wavelet surface at the proper scale, or from the original time data using the hop time parameters.

Visual inspection of the wavelet surfaces permits the identification of FH signals at SNR levels of 3 dB and above. Other modulation schemes such as ASK, PSK, and MFSK will only have cellular patterns on one of the wavelet surfaces, that is their frequency bandwidth does not span more than one wavelet scale. Hop timing estimation shows that the hop start/stop times can be estimated with an accuracy of 12 to 17.5 per cent at SNR levels of 6 dB or better.

The performance of longer duration wavelets is better than that of shorter ones since longer wavelets have better spectral energy concentration than shorter ones. The success rate of frequency estimation from the wavelet surfaces showed that the probability of correct frequency estimation from the wavelet surface is 1.0 for input SNR's of 0 dB and above. A frequency estimation success rate of 1.0 requires an SNR level of -3 dB or about -3 dB to -5 dB using the time data directly or wavelet surfaces, respectively. The minimum SNR required for an automated estimation of hop times is 6 dB.

Processing along the time axis allows detection of the transition times of frequency and time hopped signals. The current implementation is limited to work with one transition per observation interval but permits robust detection at an SNR of 3 dB.

7.2   RECOMMENDATIONS FOR FUTURE WORK

There are other ways to define or estimate the instantaneous (or temporal) correlation function. A study to evaluate different candidate ICS (or TCS) should be performed.

For processing of the ICS along the delay axis we recommend the following:

i) Refine the automatic recognition of the cellular structure of the FH signal over the wavelet surfaces.

ii) Improve the performance of the hop-scale identification at lower SNR by reexamining the equalization of the spectrum of the ICF surfaces.

iii) Investigate other wavelet types, and the use of other definitions for the instantaneous correlation function.

iv) Combine information from different wavelet surfaces to improve parameter estimation.

For processing the ICS along the time axis we recommend investigation of extensions for successful operation when more than one transition (jump) is present during the observation interval.

Finally, both approaches, transformation over time and delay, will benefit from an improved edge detection scheme. This problem should be addressed in more detail.

Bibliography

[1] Gardner, W. A., "Signal Interception: A Unifying Theoretical Framework for Feature Detection," IEEE Trans. on Communication, Vol. 36, No. 8, pp. 897-906, Aug. 1988.

[2] Gardner, W. A., "Spectral Correlation of Modulated Signals: Part II- Digital Modulation," IEEE Trans. on Communications, Vol. Com-35, No. 6, June 1987.

[3] Reichert, J., "Automatic Classification of Communication Signals Using Higher Order Statistics," ICASSP-92, Vol. 5, pp.221-224, San Francisco, Mar. 1992.

[4] Goh, T. T., Liu, J., and Soong, B. H., "Deterministic Signal Detection:A Hybrid Approach," Communication on the Move, Singapore, ICCS/ISITA , Vol. 1, pp. 385-389, 1992.

[5] Hippenstiel, R. D., and Fargues, M. P., "Feature Extraction from Digital Communication Signals Using Wavelet Transform," Naval Postgraduate School Technical Report No. NPS-EC-95-001, Feb. 1995.

[6] Wei, W., and Mendel, J. M., "A New Maximum Likelihood Method for Modulation Classification," 29th Asilomar Symposium on Signals, Systems and Computers, Vol. 2, pp. 1132-1136, 1995.

[7] Fonollosa, J. R., and Nikias, C. L., "Analysis of QAM Signals Using Higher-Order Spectra Based Time-Frequency Distributions," IEEE Signal Processing Workshop on High-Order Statistics, pp. 225-229, South Lake Tahoe, CA, 1993.

[8] Vergara, L., Borrallo, J. M., Garcia, J. P., and Mezcua, B. R., "A General Approach to the Automatic Classification of Radio Communication Signals," Signal Processing, Vol. 22, pp. 239-250, 1991.

[9] Lin, Y., and Jay Kuo, C-C., "Sequential Modulation Classification of Dependent Samples," ICASSP-96 , Vol. 5, pp. 2690-2693,Atlanta, 1996.

[10] Kim, K., and Polydoros, A., "Digital Modulation Classification: The BPSK versus QPSK case," MILCOM 88, pp. 431-436, 1988.

[11] Gardener, W., "The Role of Spectral Correlation in Design and Performance Analysis of Synchronizers," IEEE Trans. on Communications, Vol. Com-35, No. 11, Nov. 1987.

[12] Wickert, M. A., and Turcotte, R. L., "Rate-Line Detection Using Higher-Order Spectra," MILCOM'92, Communication-Fusing Command, Control, and Intelligence, Vol. 3, pp. 1221-1225, 1992.

[13] Chuan, Y., and Jay Kuo, C., "Modulation Classification Using Wavelet Transform," Proc. of SPIE, Wavelet Application in Signal and Image Processing II, Vol. 2303, pp. 260-271, 1994.

[14] Marinovich, N., Nelson, D., Cohen, L., and Umesh, S., ``Classification of digital modulation types," SPIE, Vol. 2563, pp. 126-143, 1996.

[15] Roessgen, M., and Boashash, B., ``Time-Frequency Peak Filtering Applied to FSK Signals," Proc. of IEEE-SP International Symp. on Time-Frequency and Time-Scale Analysis, Philadelphia, Oct. 1994.

[16] Garcia, F. M., and Lourtie, I. M., ``A Wavelet Transform Frequency Classifier For Stochastic Transient Signals," IEEE ICASSP-96, Vol. 6, pp. 3057-3060, 1996.

[17] Hippenstiel, R., and Fargues, M., ``Feature Extraction from Digital Communication Signals Using Wavelet Transform," 29th Asilomar Symposium on Signals, Systems and Computers, Vol. 1, pp. 285-289, 1995.

[18] Reappaport, S. S., and Grieco, D. M., ``Spread Spectrum Signal Acquisition: Methods and Technology," IEEE Communication Magazine, Vol. 22, No. 6, June 1984.

[19] Simon, M., Omura, J., Scholtz, R, and Levitt, B, Spread Spectrum Communication Systems, Computer Science Press, Vol. III, Ch. 4, 1985.

[20] Krasner, N., ``Optimal Detection of Digitally Modulated Signals," IEEE Trans. on Communications, Vol. Com-30, No. 5, May 1982.

[21] Polydoros, A., and Weber, C.L., ``Detection Performance Consideration for Direct-Sequence and Time-Hopping LPI Waveform," IEEE J. on Selected Areas of Communications, SAC-3, pp. 727-744, Sep. 1985.

[22] Beaulieu, N., Hopkins, W., and McLane, P., ``Interception of Frequency-Hopped Spread Spectrum Signals," IEEE J. on Selected Areas of Communications}, SAC-8, pp. 853-870, June 1990.

[23] Chung, C. D., ``Generalized Likelihood-Ratio Detection of Multiple-Hop Frequency-Hoping Signals," IEE Proc. Communications, Vol. 141, Iss: 2, pp. 70-78, Apr. 1994.

[24] Dillard, R. A., and Dillard, G. M., ``Likelihood-Ratio Detection of Frequency-Hopped Signals," IEEE Trans. on Aerospace and Electronic Systems, Vol. 32. pp. 543-553, Apr. 1996.

[25] Nemisick, L. W., and Geraniotis, E., ``Adaptive Multichannel Detection of Frequency-Hopping Signals," IEEE Trans. on Communications, Vol. 40, No. 9, Sep. 1992.

[26] Nemisick, L. W., and Geraniotis, E., ``Detection of Frequency Hopping Signals via Adaptive Multichannel Radiometry," IEEE MILCOM-92, Communication, Fusing Command, Control and Intelligence, Vol.3, pp. 1215-1220, 1992.

[27] Chung, C. D., and Polydoros, A., ``Detection and Hop-Rate Estimation of Random FH Signals via Autocorrelation Technique," MILCOM-91, Communication in a Changing World , Vol. I, pp. 345-49, Nov. 1991.

[28] Aydin, L., and Polydoros, A., ``Hop-Timing Estimation for FH Signals Using a Coarsely Channelized Receiver," IEEE Trans. on Communications, Vol. 44, pp. 516-5226, April 1996.

[29] Mauck, K. D., and Betz, J. W., ``Quadratic Extraction of Feature from Direct Sequence Signals," Mitre Technical Report, Bedford, MA, 1991.

[30] Kuehls, J. F., and Geraniotis, E., ``Presence Detection Of Binary-Phase-Shift-Keyed and Direct-Sequence Spread Spectrum Signals Using a Prefilter-Delay-and-Multiply Device," IEEE J. on Selected Areas in Communication, Vol. 8. No. 5. June 1990.

[31] Mammone, R. J., Rothaker, R. J., Podilchuk, C. I., Davidvici, S., and Schilling, D. L.,``Estimation of Carrier Frequency, Modulation Type and Bit Rate of an Unknown Modulated Signal," IEEE International Conf. on Communications 87, Vol.2, pp. 1006-1012, Seattle, WA, June 7-10, 1987.

[32] Ho, K. C., Prokopiw, W., and Chan, Y. T.,``Modulation Identification by the Wavelet Transform ," MILCOM-95, Vol. 2, No. 2/3/4, pp. 886-890, Nov. 1995.

[33] Chung, C. D., and Polydoros, A., ``Parameter Estimation of Random FH Signals Using Autocorrelation Techniques," IEEE Trans. on Communications, Vol. 43, No.2/3/4, pp. 1097-1106, Feb./Mar./Apr. 1995.

[34] Kimble, K. R., and Tibbals, T. F., ``Spectral Analysis Techniques Using Wavelets as an Alternative to Fourier Analysis For Transient Dynamic Data," Arnold Engineering Development Center Final Technical Report, AEDC-TR-94-17, Jan. 1995.

[35] Cochran, D., ``Application of Wavelet Transform Techniques to Spread Spectrum Demodulation and Jamming," Air Force Office of Scientific Research Final Technical Report, TRC DC-9302, Feb. 1993.

[36] Proakis, J. D., and Manolakis, D. G., Digital Signal Processing, Principles, Algorithms, and Applications, Prentice Hall, Inc., Englewood Cliffs, NJ, 1996.

[37] Akansu, A. N., and Haddad, R. A., ``Multiresolution Signal Decomposition," Academic Press Inc., 1992.

[38] Cohen, L., Time-Frequency Analysis, Prentice-Hall Inc., Inglewood Cliffs, NJ, 1995.

[39] Classen, T., and Mecklenbrauker, W., ``The Wigner Distribution: A Tool for Time-Frequency Signal Analysis, Part I: Continuous-Time Signal," Philips J. of Research, Vol. 35, pp. 271--250, 1980.

[40] Classen, T., and Mecklenbrauker, W., ``The Wigner Distribution: A Tool for Time-Frequency Signal Analysis, Part II: Discrete-Time Signal," Philips Journal of Research, Vol. 35, pp. 276--300, 1980.

[41] Hill, R. O., Elementary Linear Algebra with Applications, Harcourt Brace Jovanovich Press, 1991.

[42] Daubechies, I., Ten Lectures on Wavelet, SIAM, 1992.

[43] Kaiser, G., A Friendly Guide to Wavelets, Birkhauser, 1995.

[44] Rioul, O. L., and Vetterli, M., `` Wavelets and Signal Processing," IEEE Signal Processing Magazine, Oct. 1991.

[45] Vetterli, M., and Herley, C., ``Wavelet and Filter Banks: Theory and Design", IEEE Trans. on Signal Processing, Vol. 40, No. 9, Sep. 1992.

[46] Strang, G. and Nguyen, T., Wavelet and Filter Banks, Wellesly-Cambridge Press, 1996.

[47] Burrus, C. S., Gopinath, R. A., and Guo, H., Introduction to Wavelets and Wavelet Transforms, Prentice-Hall, Englewood Cliffs, NJ, 1998.

[48] Drumheller, `` Theory and Application of the Wavelet Analysis to Signal Processing," Naval Research Laboratory Technical Report, No.9316, July 1991.

[49] Friedlander, B., and Marple, L., Jr., ``High Performance Spectral Analysis Techniques for Non-Stationary Signals," Signal Processing Technology Ltd. Technical Report, June 1995.

[50] Peterson, R., Ziemer, R., and Borth, D., Introduction to Spread Spectrum Communications, Prentice-Hall, Inc., Englewood Cliffs, NJ, 1995.

[51] Couch, L. W., Digital and Analog Communication Systems, Macmillan Publishing Company, 1990.

[52] Papoulis, A., Probability, Random Variables and Stochastic Processes, 3rd ed., McGraw-Hill, Inc., New York, 1991.

[53] Whalen, A. D., Detection of Signals in Noise, Academic Press Inc., 1970.

[54] Abramowitz, M, and Stegun, I. A., Handbook of Mathematical Functions, Dover Publications, Inc., 1970.

[55] Gradshteyn, I.S., and Ryzhik, I.M., Table of Integrals, Series, and Products, 5th ed., Academic Press Inc., 1994.

[56] Khalil, Nabil H., "Wavelet Analysis of Instantaneous Correlations with Applications to Frequency Hopped Signals", Ph. D. Dissertation, Naval Postgraduate School, Sept. 1997.

[57] Helstrom, C. W., Probability and Stochastic Processes for Engineers, Macmillan, New York, 1991.

[58] Spiegel, M. R., Mathematical Handbook of Formulas and Tables, 32nd ed., McGraw-Hill, Inc., 1994.

[59] Misiti, M., Misiti, Y., Oppenheim, G., and Poggi, J., Wavelet Toolbox User's Guide, The Mathworks Inc., 1996.

[60] Lina, J., and Mayrand, M., `` Complex Daubechies Wavelets", UdeM-Physnum-ANS-15, Dec. 1993.

[61] Kay, S. M., Modern Spectral Estimation Theory and Application, Prentice-Hall, Englewood Cliffs, NJ, 1988.

[62] Jain, A. K., Fundamentals of Digital Image Processing , Prentice-Hall, Englewood Cliffs, NJ, 1990.

[63] Overdyk, Howard F.," Detection and estimation of frequency hopping signals using wavelet transforms," MSEE Thesis, Naval Postgraduate School, Sept. 1997.

[64] M. Simon, U. Cheng, L. Aydin, A. Polydoros, and B. Levitt, "Hop timing estimation for non-coherent frequency hopped M-FSK intercept receivers, IEEE Trans. Commun., Vol. 43, pp. 1144-1154, 1995.

INITIAL DISTRIBUTION LIST

		No. Copies
1.	Defense Technical Information Center 8725 John J. Kingman Rd, STE 0944 Ft. Belvoir, VA 22060-6218	2
2.	Dudley Knox Library, Code 52 Naval Postgraduate School 411 Dyer Road Monterey, CA 93943-5101	2
3.	Research Office, Code 09 Naval Postgraduate School 589 Dyer Road Monterey, CA 93943-5138	1
4.	Chairman, Code EC Department of Electrical and Computer Engineering Naval Postgraduate School 833 Dyer Road Monterey, CA 93943-5121	1
5.	Professor Ralph D. Hippenstiel, Code EC/Hi Department of Electrical and Computer Engineering Naval Postgraduate School 833 Dyer Road Monterey, CA 93943-5121	4
6.	Professor Monique P. Fargues, Code EC/Fa Department of Electrical and Computer Engineering Naval Postgraduate School 833 Dyer Road Monterey, CA 93943-5121	2
7.	David Korn, WF4/I2PO ISC 4101 Pleasant Valley Road Chantilly, VA 20151	3